photonics

MDPI

Review

Advances in Versatile Light Field Manipulation with On-Chip Metasurfaces

Yilan Pang [1], Jiaqi Cao [1,2], Sitong Lin [1], Meng Wang [1,2], Xin Liu [1,2], Tianqi Zhao [1] and Bin Fang [1,2,*]

[1] College of Optical and Electronic Technology, Zhejiang Province Key Laboratory of Optoelectronic Metrology and Precision Instruments, China Jiliang University, Hangzhou 310018, China
[2] Centre for THz Research, China Jiliang University, Hangzhou 310018, China
* Correspondence: binfang@cjlu.edu.cn

Abstract

The relentless pursuit of higher information density and processing speed has driven photonic chips toward miniaturization, high performance, and multifunctional integration. Metasurfaces, composed of subwavelength artificial meta-atoms, have emerged as a revolutionary platform for manipulating light fields at the nanoscale, offering unprecedented control over amplitude, phase and polarization, as well as enabling frequency conversion through nonlinear processes. When seamlessly integrated with on-chip optical waveguides, metasurfaces provide a compelling solution for bridging guided waves and free-space waves, enabling compact, high-performance photonic devices with versatile light-manipulation capabilities. This review systematically surveys recent advances in on-chip metasurfaces for multifunctional light field manipulation, with a focus on guided-wave radiation control. We first elucidate the fundamental phase modulation mechanisms that collectively constitute a versatile toolbox for tailoring light fields at subwavelength scales. We then examine the three core application scenarios that define the operational framework of metasurface-integrated photonic systems: free-space-to-chip coupling, in-plane guided-wave manipulation, and guided-wave-to-free-space radiation. For each scenario, we highlight representative device architectures and their performance characteristics, tracing the evolution from single-mechanism modulation to multidimensional multiplexing and dynamic reconfigurability. We conclude by discussing remaining challenges including efficiency, dynamic tunability, and scalable fabrication, and outline future directions such as intelligent inverse design, on-chip quantum metasurfaces, and optical computing.

Keywords: light field manipulation; on-chip metasurfaces; integrated photonics; guided-wave radiation; multidimensional multiplexing; dynamic wavefront manipulation

Check for updates

Received: 31 August 2026
Revised: 22 September 2026
Accepted: 23 September 2026
Published: 26 September 2026

Copyright: © 2026 by the authors. Licensee MDPI, Basel, Switzerland. This article is an open access article distributed under the terms and conditions of the Creative Commons Attribution (CC BY) license.

1. Introduction

Photonic integrated technology has become a critical focus in the post-Moore's Law era due to its substantial capabilities in enabling high-density information processing, high-speed communication, and advanced sensing applications [1–6]. Representative integrated photonic platforms, such as silicon photonics, enable the high-density integration of active and passive components (including light sources, modulators, waveguides, and detectors) onto a single chip [7–9]. This facilitates the generation, transmission, and processing of optical signals, leading to substantial improvements in system performance, stability, and energy efficiency. However, conventional integrated photonic devices primarily rely on

components based on adiabatic waveguide structures [10,11], such as directional couplers, microring resonators, and grating couplers [12,13]. The functionality of these components often depends on optical interference and resonance effects, which typically results in millimeter-scale footprints. Furthermore, they offer limited flexibility in manipulating the degrees of freedom of light fields [14–17], such as phase, amplitude, polarization, and orbital angular momentum, making it challenging to achieve complex, multi-dimensional, and highly efficient on-chip light field control.

The recent advent of metasurfaces, a class of two-dimensional planar optical materials composed of subwavelength-scale artificial atoms arranged in specific sequences, has provided a revolutionary tool for light field manipulation [18–24]. By meticulously designing the geometry, size, orientation, and other parameters of each meta-atom, arbitrary control over the wavefront (including its phase, amplitude, and polarization) can be achieved within a subwavelength thickness. This enables a series of novel optical functionalities, such as beam steering [25–27], metalenses [28–32], holographic imaging [33–36], frequency conversion [37–41], and sensing detection [42–45]. The integration of this powerful free-space light field control capability with mature photonic integrated circuits (PICs) has given rise to the emerging interdisciplinary research field of "on-chip metasurfaces" [46,47].

The core concept of on-chip metasurfaces is to employ metasurfaces as versatile "on-chip planar optical elements" within photonic systems, allowing them to work synergistically with traditional waveguide structures to achieve efficient and flexible control of light between free-space and waveguide modes, as well as among the waveguide modes themselves [48,49]. This paradigm offers a novel pathway to address the bottlenecks of conventional integrated photonics in areas such as three-dimensional light field manipulation, mode-field matching, and multi-functional integration [50–54]. Specifically, the research scope can be systematically classified into three categories, including input meta-couplers, in-plane manipulators and guided-wave radiators, as shown in Figure 1. As interface couplers, on-chip metasurfaces can overcome the high-order diffraction loss and large footprints constraints of traditional grating couplers, enabling highly efficient and multi-functional coupling of light from free-space into specific waveguide modes [55–58]. This provides superior solutions for interconnecting chips with the external world. As in-plane manipulators, metasurfaces integrated atop waveguides can interact directly with guided modes, enabling the conversion, routing, and modulation of these modes. This allows for the implementation of compact in-plane devices like mode converters [59–61], mode (de)multiplexers [62,63], on-chip neural network [64–67] and programmable photonic circuits [68]. As guided-wave radiators, on-chip metasurfaces can replace traditional output gratings to radiate guided wave into free-space while simultaneously imposing precise wavefront control. This directly enables advanced optical functions on-a-chip, such as beam steering [69–71], focusing [72–75], holography [76–78], displays [79–83], encrypted storage [84,85], and structured light field generation [86–88], significantly expanding the optical output capabilities of photonic chips.

This review systematically outlines recent research progress in on-chip metasurfaces for light field manipulation, centered around the three core aspects above. We will first elucidate the fundamental working principles and design methodologies. Subsequently, we will delve into innovative designs and remarkable performances achieved in the three scenarios of on-chip light coupling, in-plane guided-wave manipulation, and guided-wave radiation control. Finally, we will discuss the current challenges and future opportunities for this technology, aiming to provide a technical overview of this vibrant frontier and stimulate its application in high-performance optical computing, LiDAR, quantum information processing, and compact optical sensing.

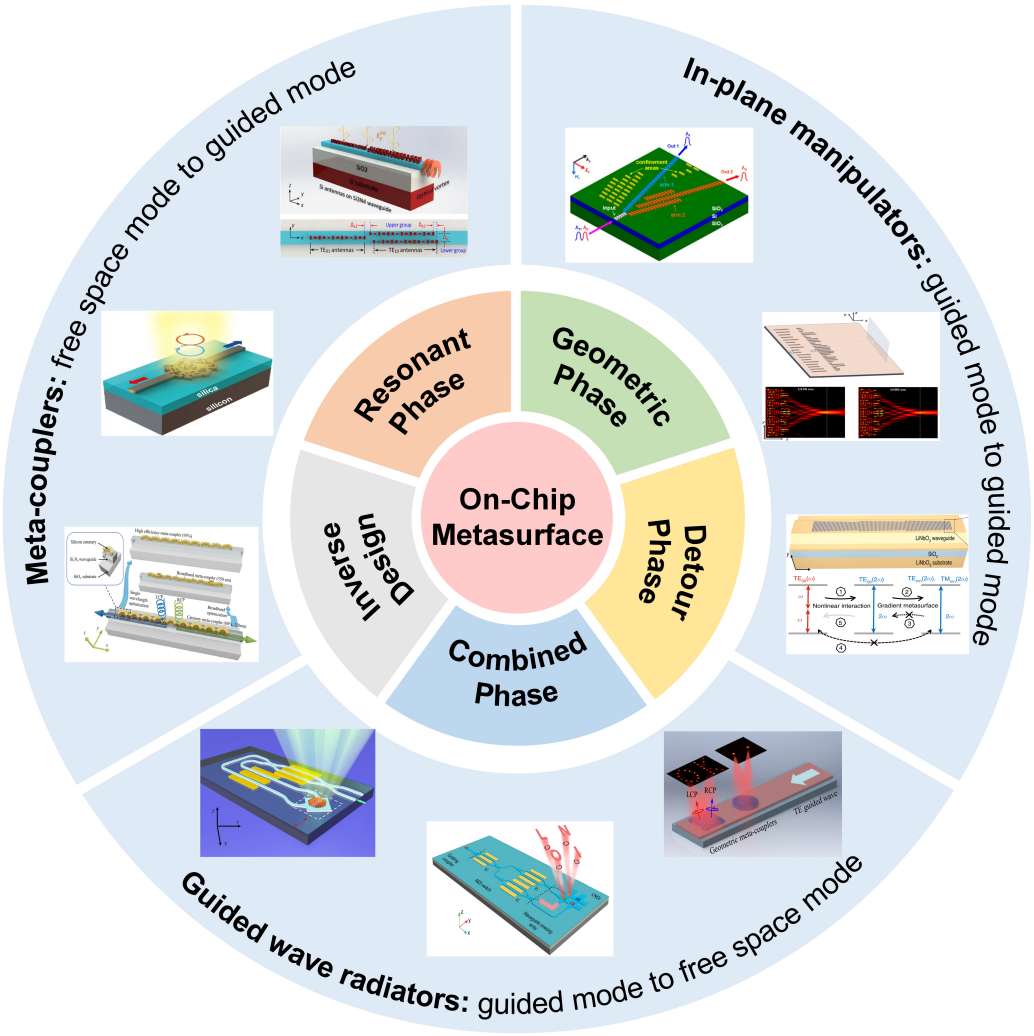


Figure 1. Versatile light field manipulation facilitated by on-chip metasurfaces encompasses multi-functional light coupling, in-plane mode modulation, and guided-wave radiation control.

2. Design Principles of On-Chip Metasurfaces

Similar to free-space metasurfaces, the mechanisms for on-chip metasurface light field manipulation primarily include resonant phase, geometric phase, detour phase, and hybrid modulation combining multiple phase mechanisms.

Resonant phase modulation involves tuning the geometric dimensions of the meta-surface unit cells to alter their internal localized resonance modes, thereby achieving a 2π phase coverage, as illustrated in Figure 2a. While reliance on variations in nanostructure shape or size offers greater design freedom, achieving full 2π phase coverage often requires complex parameter scanning or optimization processes. Furthermore, resonant phase is sensitive to wavelength, typically resulting in a narrow operating bandwidth and imposing high demands on fabrication precision.

Geometric phase (also known as the Pancharatnam–Berry phase, PB phase) operates by rotating the central orientation angle of the metasurface unit cells, as shown in Figure 2b. Under circularly polarized light incidence, it provides an additional phase shift equal to twice the rotation angle for the converted cross-polarized output light. Since geometric phase modulation depends solely on the rotation angle of the units, it offers relative simplicity in structural design and fabrication processes. It is also wavelength-insensitive, granting it broadband and robust characteristics. However, geometric phase is inherently limited to responding only to circularly polarized light and lacks decoupling of phase for

left- and right-handed circular polarizations (LCP/RCP), which restricts the multiplexing capability of wavefront manipulation functions.

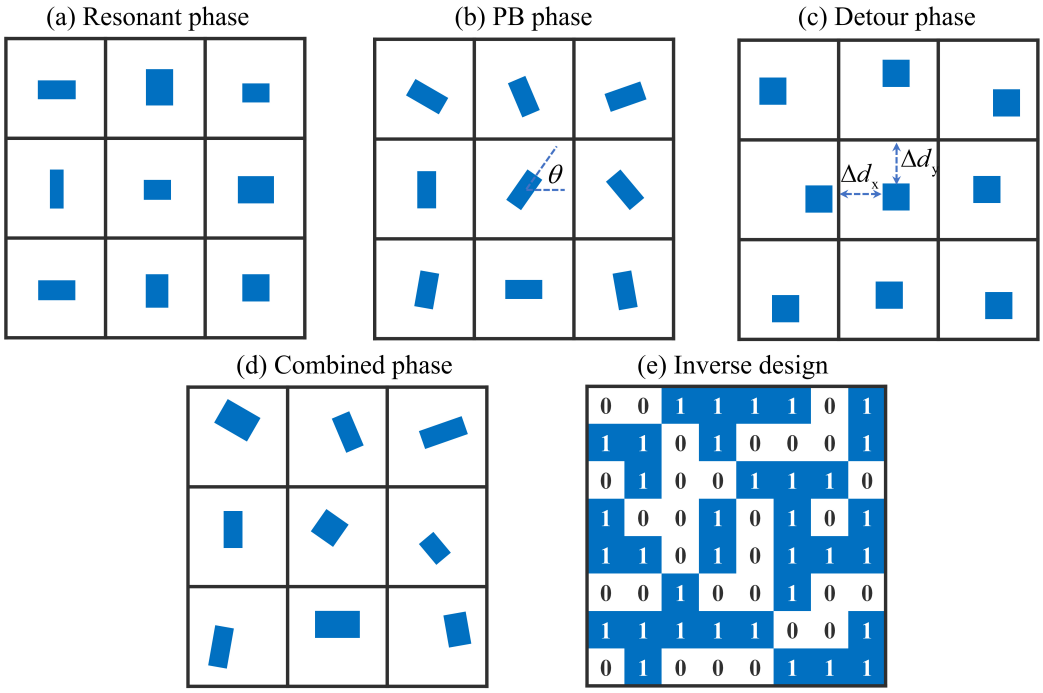


Figure 2. Fundamental phase modulation mechanisms of on-chip metasurfaces for light field manipulation. (**a**) Resonant phase; (**b**) Geometric phase; (**c**) Detour phase; (**d**) Hybrid modulation strategy combining multiple phase mechanisms; (**e**) Inverse design approach utilizing algorithm-driven optimization to generate complex two-dimensional subwavelength structures.

Detour phase introduces an additional phase delay, $\Delta\varphi = 2\pi\Delta d/p$, by laterally shifting the metasurface structure within a unit cell period by Δd, where p is the period of the metasurface along the x (or y) direction, as depicted in Figure 2c. This modulation mechanism is independent of the resonant modes or material dispersion of the metasurface. Phase coverage from 0 to 2π can be achieved merely through positional offset, and it allows for independent control along orthogonal directions with low cross-talk between channels. This provides extra design freedom for independently manipulating multiple optical parameters (e.g., amplitude, polarization, and phase). However, devices based on detour phase exhibit strong wavelength dependence, which limits their performance in broadband applications.

Although single-phase mechanisms can manipulate the wavefront, they often struggle to simultaneously meet the demands of complex light field control for bandwidth, efficiency, and multifunctionality. Therefore, hybrid modulation strategies combining multiple mechanisms are typically employed, as shown in Figure 2d. This approach leverages the advantages of each mechanism while increasing the degrees of freedom in light field manipulation, thereby enriching and enhancing device functionality and performance.

Beyond conventional modulation mechanisms, algorithm-driven optimization can be used to design complex two-dimensional subwavelength structures that are difficult to conceive through intuitive traditional methods, further expanding the functionality and performance of on-chip metasurfaces, as illustrated in Figure 2e. This design process for such "disordered" metasurfaces is often termed "inverse design" [62,63]. It fundamentally differs from the traditional design approach (from structure to simulation and then to performance). Instead, starting from the desired functionality, algorithms automatically search for the optimal structural realization, completely breaking away from the framework of

traditional periodic metasurfaces. Consequently, this generalized concept of metasurfaces provides new avenues for on-chip light field manipulation [89–91].

To evaluate different mechanisms, a comparison is summarized in Table 1. For free-space-to-chip couplers, the primary requirements are high coupling efficiency, broadband operation, and controllable polarization or spin selectivity. Hybrid modulation combining geometric and detour phases, or inverse design, is often preferred because it can simultaneously satisfy phase-matching, polarization decoupling, and broadband operation. For in-plane mode converters, high mode purity and low inter-channel crosstalk are critical. Detour phase and hybrid modulation are attractive owing to their independent control along orthogonal directions and low crosstalk. For holographic displays and multidimensional multiplexing of guided wave radiation control, geometric phase provides spin selectivity, detour phase offers wavelength- and direction-dependent encoding, and resonant phase adds wavelength selectivity. Hybrid modulation or inverse design is therefore the most effective route to achieve polarization, wavelength, direction, and diffraction-order multiplexing.

Table 1. Comparison of phase-modulation mechanisms for on-chip metasurfaces.

Mechanism	Phase Coverage Method	Polarization Dependence	Bandwidth	Fabrication Complexity	Decoupling Capability
Resonant	Geometric dimensions	Designable	Narrowband	High	Weak
Geometric	Rotating anisotropic meta-atoms	Spin dependent	Broadband	Low	Weak
Detour	Lateral displacement within a unit cell	Designable	Narrowband	Moderate	Good
Combined	Combining two or more mechanisms	Designable	Designable	Moderate to high	Strong
Inverse design	Algorithm-driven optimization	Designable	Designable	High	Strong

3. Free-Space Light Coupling with On-Chip Metasurfaces

Efficiently coupling free-space light into on-chip waveguides or microcavities is crucial for achieving high-performance photonic devices and large-scale integrated optical circuits. Early on, researchers commonly used optical fibers or prisms for coupling [92,93]. However, such methods often relied on precise mechanical alignment and complex optical setups, which greatly limited the application potential of integrated systems. Another common approach, grating coupling [94,95], typically requires incident light at a specific angle, making it difficult to adapt to divergent beams. Moreover, its efficiency is quite sensitive to the polarization state and wavelength of the light, which is unfavorable for broadband, polarization-independent integrated applications. In contrast, on-chip metasurface-based couplers demonstrate numerous advantages [96–100]. In 2017, Gong et al. demonstrated a hybrid unidirectional meta-coupler based on a plasmonic metasurface composed of metal–insulator–metal unit cells [101]. By leveraging the phase gradient to provide an in-plane wavevector via the generalized Snell's law, they achieved highly efficient and unidirectional coupling of normally incident light into a high-index waveguide (e.g., silicon nitride), exciting the fundamental transverse electric (TE_0) mode. In the same year, Guo et al. demonstrated a waveguide-integrated plasmonic nanoantenna capable of polarization-selective and mode-selective directional coupling [102]. By combining two pairs of gold nanorods with different lengths and orientations on a silicon rib waveguide, the device routed horizontally polarized free-space light into the right-propagating TM mode and vertically polarized light into the left-propagating TE mode, thereby functioning

as an ultra-compact polarization demultiplexer, as shown in Figure 3a. Building on this, Lin et al. in 2018 designed a silicon fishbone nanoantenna array integrated on a standard 220 nm silicon-on-insulator (SOI) platform, functioning as a compact on-chip circular polarization splitter [103]. This device resolved incident circular polarization states and directly routed left- and right-handed circularly polarized light into separate single-mode silicon waveguides, representing a significant advance toward chip-scale manipulation and detection of spin angular momentum.

Subsequently, in 2019, Zhang et al. integrated an all-dielectric metasurface composed of elliptical silicon nanopillars onto a silicon nitride waveguide, demonstrating spin-selective directional coupling and wavelength demultiplexing [104]. The phase gradient provided by the metasurface satisfied the phase-matching condition, while the strategic placement of the nanoantennas at the waveguide's chiral points exploited the spin–momentum locking effect for directional control. Moreover, by tailoring the geometric parameters, the device could route light of different wavelengths to distinct propagation directions and waveguide modes, thereby functioning as a wavelength demultiplexer. In 2020, Meng et al. proposed a more universal design strategy by synergizing the Jones matrix model with the generalized Snell's law under the phase-matching framework, achieving versatile on-chip light coupling with full control over coupling direction, operating wavelength, and excited waveguide mode for arbitrary incident polarizations [105], as shown in Figure 3b. They further demonstrated a chip-integrated vortex beam generator that converted free-space linearly polarized light into a waveguide mode carrying orbital angular momentum, significantly expanding the functional capabilities of on-chip couplers. In contrast to conventional forward-design approaches, Xie et al. employed inverse design on a standard SOI platform to realize a compact, broadband photonic spin Hall metasurface coupler with a footprint of only 2.4 μm in diameter [106], as shown in Figure 3c. This device acted simultaneously as a spin detector and emitter, separating incident left- and right-handed circularly polarized light into opposite waveguide arms with an experimentally measured extinction ratio exceeding 20 dB over an 80 nm bandwidth (1528–1608 nm) and a simulated 3 dB bandwidth exceeding 200 nm. This inverse-designed, non-intuitive structure overcame the limitations of previous spin-sorting devices—namely low efficiency or narrow bandwidth—providing a high-performance, broadband solution for on-chip spin manipulation in quantum information processing and optical communications. Recently, Chen et al. also demonstrated a free-form catenary-inspired meta-coupler that simultaneously achieves ultra-high coupling efficiency and broad bandwidth by employing an adjoint-based topology optimization strategy [107], as shown in Figure 3d. By customizing the near-field distribution to suppress spurious diffraction orders and destructive interference between adjacent meta-atoms, they achieved a maximum coupling efficiency of 93% with an extinction ratio of 16.7 dB at 1550 nm, as well as a broadband meta-coupler covering the O- to L-bands with over 350 nm bandwidth and 50% average coupling efficiency, as shown in Figure 3d.

Beyond linear optics, Fang et al. extended the functionality of metasurfaces from linear to nonlinear optics, demonstrating their power as couplers and in-plane nonlinear processors [108]. As depicted in Figure 3e, they designed a grating metasurface on the lithium niobate (LN) waveguide to achieve phase matching for second-harmonic generation from a free-space 1064 nm pump to a guided 532 nm second-harmonic wave. Through holographic encoding on the metasurface, they demonstrated independent control over the intensity and phase of the generated second-harmonic wave, and experimentally realized multiple beam-shaping functions including single- and dual-focusing as well as direct generation of Airy beams within the waveguide. This work integrates nonlinear frequency conversion and beam manipulation into a single compact device, highlighting the potential of metasurface-integrated lithium niobate waveguides for on-chip nonlinear photonics and

multichannel optical routing. In summary, employing on-chip metasurfaces as couplers, it not only achieves high-efficiency coupling and more compact device sizes, but also enables flexible coupling of free-space optical fields with arbitrary wavefronts into specific waveguide modes, as presented in Table 2, providing a highly efficient and versatile optical interface solution for integrated photonics.

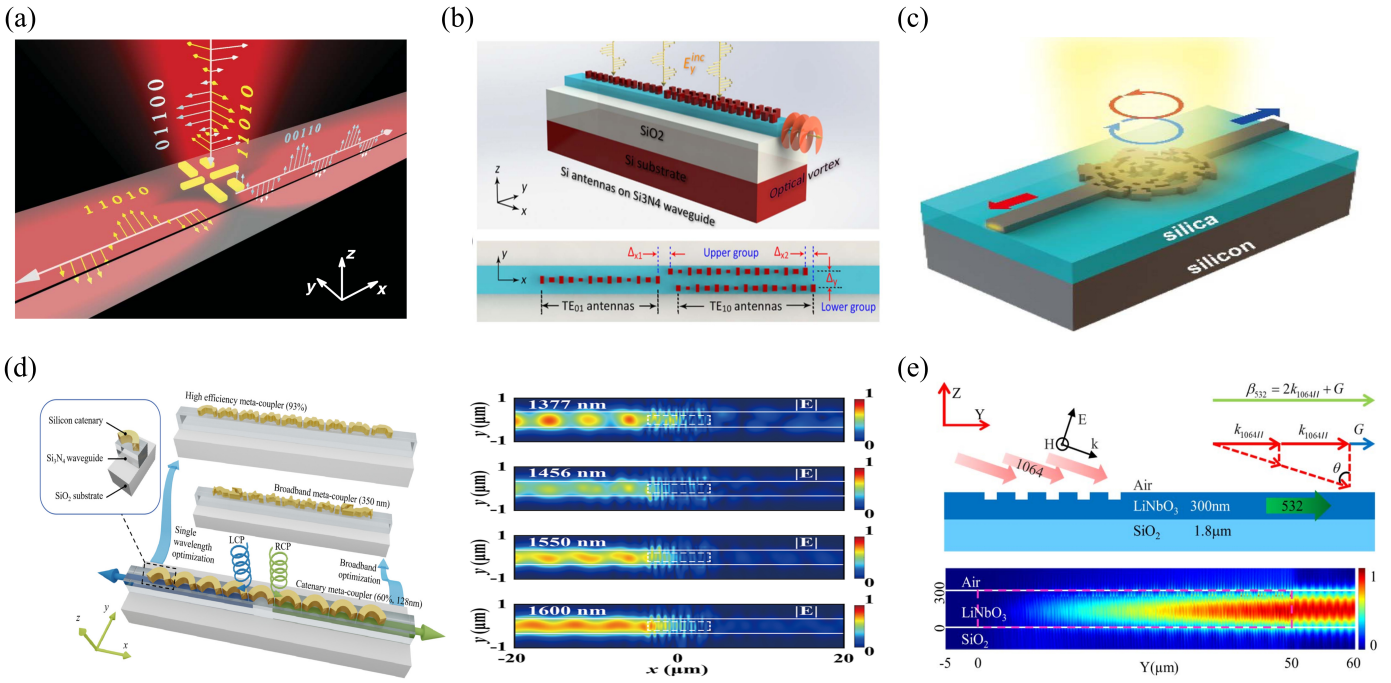


Figure 3. Versatile on-chip light coupling with metasurface. (**a**) High–bit rate ultra-compact light routing with mode-selective on-chip nanoantennas. Reprinted from [102] under a Creative Commons Attribution NonCommercial License 4.0 (CC BY-NC). Copyright © 2017 The Authors; (**b**) Versatile light coupling and (**d**,**e**) multiplexing from arbitrary polarizations to controlled waveguide modes using dielectric metasurface [105]; (**c**) Broadband spin-dependent light separation via inverse design on-chip metasurface [106]; (**d**) Free-form catenary-inspired meta-couplers for ultra-high or broadband vertical coupling [107]; (**e**) Integrating light coupling, frequency conversion, and nonlinear beam engineering into a single grating metasurface [108].

Table 2. Comparison of representative free-space-to-chip metasurface couplers (Section 3).

Ref.	Phase Mechanism	Tunable Dimensions	Efficiency /Bandwidth	Footprint	Static/ Dynamic
[101]	Resonant phase	/	/		Static
[102]	Resonant phase	Polarization, mode	/	Ultra-compact	Static
[103]	Geometric phase	spin	/	compact	Static
[104]	Geometric phase	Spin, wavelength	/		Static
[105]	Combined phase	Arbitrary polarization, wavelength, waveguide mode	/	/	Static
[106]	Inverse design	Spin	Extinction ratio > 20 dB over 80 nm (1528–1608 nm); simulated 3 dB bandwidth > 200 nm	2.4 μm diameter	Static
[107]	Inverse design	Spin	Max 93%; extinction ratio 16.7 dB at 1550 nm; O-to-L band > 350 nm, 50% average	/	Static
[108]	Detour phase	Wavelength (1064 → 532 nm), beam shape	/	compact	Static

4. In-Plane Mode Manipulation with On-Chip Metasurfaces

By utilizing on-chip integrated metasurfaces, it becomes possible not only to couple free-space light into waveguides but also to achieve in-plane manipulation of guided-wave modes, enabling versatile functionalities such as mode conversion [109–111], beam splitting or routing [112–117], wavefront shaping [118–124] and frequency conversion [125].

In 2016, Ohana et al. established an early paradigm for in-plane mode conversion using dielectric metasurfaces in guided-wave systems [109]. They fabricated a nanoscale dielectric metasurface atop a silicon waveguide, which provided a periodic perturbation along the propagation direction for phase matching and a graded effective index profile along the transverse direction for mode overlap. The device successfully performed high-purity conversion from the TE_0 to the TE_1 mode with a measured mode purity of ~95%, while maintaining a high transmission of ~88% relative to an unperturbed waveguide. This work demonstrated that metasurfaces, grounded in effective medium theory, could serve as a robust and efficient platform for exciting and converting different eigenmodes within a waveguide. Building upon this concept, Li et al. in 2019 showed that gradient metasurfaces could offer a highly effective platform for in-plane manipulation of guided waves [110]. They experimentally realized a series of compact and broadband devices, including waveguide mode converters, polarization rotators, and structures enabling highly asymmetric optical power transmission. By leveraging a unidirectional phase gradient, these metasurfaces imparted a large collective momentum to the guided waves, enabling efficient mode conversion and control within a footprint of just a few wavelengths. The approach was successfully implemented with both gold nanorods for mid-infrared applications and low-loss silicon nanorods on lithium niobate for the telecom band, with the latter achieving negligible insertion loss. In the same year, Wang et al. designed and experimentally demonstrated an ultra-compact silicon waveguide mode converter based on an all-dielectric metasurface featuring a tilted subwavelength periodic perturbation [111]. By etching parallelogram-shaped nanostructures onto a silicon waveguide, the device enabled efficient and scalable conversion between TE modes. The researchers fabricated and characterized two converters: one for TE_0-to-TE_1 conversion with a length of 5.75 μm, and another for TE_0-to-TE_2 conversion with a length of 6.736 μm. Both devices achieved low insertion losses (<1 dB) and crosstalk below −10 dB across a 20 nm bandwidth around 1550 nm. The compact footprint and robust performance underscored the potential of dielectric metasurfaces for efficient in-plane mode manipulation in high-density integrated photonic circuits.

As shown in Figure 4a, Wu et al. demonstrated a programmable waveguide mode converter based on a phase-gradient metasurface made of the phase-change material $Ge_2Sb_2Te_5$ (GST). By exploiting the large refractive index change in GST during its phase transition, the device enabled precise control over the conversion between the TE_0 and TE_1 waveguide modes with up to 64 distinguishable levels, corresponding to 6-bit programming resolution. This programmable mode converter was further employed as a photonic computing core to construct a multimode optical convolutional neural network, successfully performing image processing and recognition tasks such as edge detection and handwritten digit classification.

Beyond mode conversion, the integration of metasurfaces with waveguides has also enabled advanced polarization handling and beam splitting. In 2015, Shen et al. demonstrated an ultra-compact polarization beamsplitter on an SOI platform using a free-form metasurface and a direct-binary-search optimization algorithm, achieving a record-small footprint of only 2.4 × 2.4 μm^2 [112]. They further designed a multifunctional variant that acted simultaneously as a polarization beamsplitter and a mode converter, efficiently coupling a multimode input waveguide to two single-mode outputs. This work highlighted

the potential of inverse-designed nanophotonics for realizing complex, multifunctional optical manipulation within an extremely compact footprint. Meanwhile, Fan et al. demonstrated an ultra-compact on-chip wavelength demultiplexer based on plasmonic metalines integrated on a silicon-on-insulator waveguide [113]. By exploiting the resonant properties of gold cut-wire nanoresonators to locally modify the effective index of the waveguide in a wavelength-dependent manner, they achieved 1.3/1.6 μm wavelength separation with an extinction ratio up to 20 dB within a footprint of only 4 μm × 4 μm, as shown in Figure 4b.

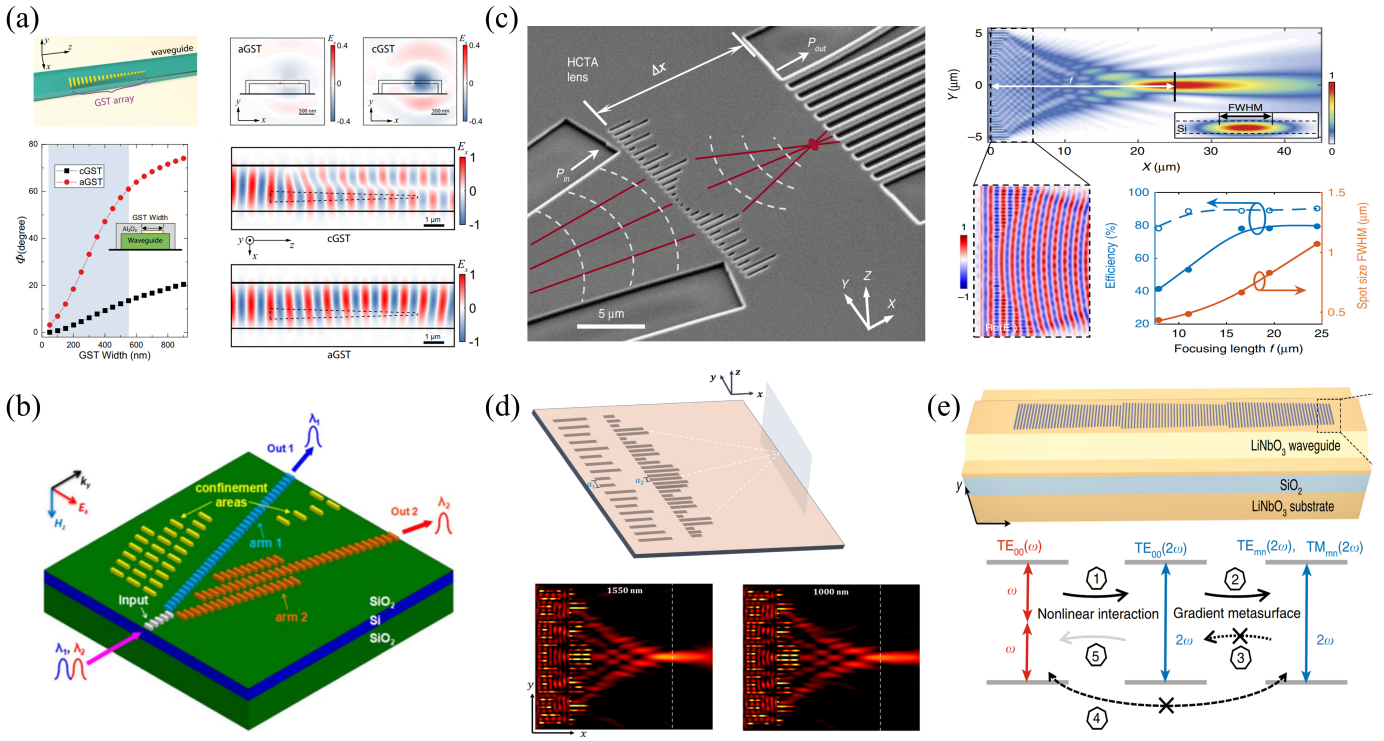


Figure 4. On-chip metasurfaces for in-plane manipulation of guided waves. (**a**) Programmable phase-change metasurfaces on waveguides for multimode photonic convolutional neural network; (**b**) Ultra compact on-chip metaline-based 1.3/1.6 μm wavelength demultiplexer [113]; (**c**) On-chip wavefront shaping with dielectric metasurface [122]; (**d**) AI-assisted on-chip nanophotonic convolver based on silicon metasurface [124]; (**e**) Gradient metasurface on lithium niobate for phase-matching-free second-harmonic generation [125].

Subsequently, Wang et al. proposed an efficient digitized adjoint method for the inverse design of chip-integrated metasurfaces [114], combining adjoint sensitivity analysis with a brute-force quantization process in three distinct stages: initial continuous topology optimization, forced permittivity biasing to create a quasi-digital pattern, and final conversion to a multilevel digital pattern. As proof-of-concept devices, they designed and fabricated a compact single-mode 3 dB power divider and a dual-mode demultiplexer. Compared to the conventional direct-binary-search brute-force method, the proposed approach achieved a fivefold improvement in design efficiency while maintaining comparable device performance.

In addition to mode management, on-chip metasurfaces have also been exploited for advanced beam shaping. As shown in Figure 4c, Wang et al. demonstrated an on-chip dielectric metasurface based on a one-dimensional metasurface defined on a standard silicon-on-insulator substrate, achieving low-loss wavefront shaping with an insertion loss below 1 dB over a 200 nm bandwidth [122]. By precisely engineering the length and width of the etched slots to control the transmitted phase and amplitude, they realized an on-chip metalens with a numerical aperture up to 2.14. Then Fan et al. developed hybrid

metasurface–waveguide platforms for in-plane beam shaping and long-range collimated propagation within integrated photonic circuits [123]. They demonstrated the generation of a two-dimensional diffraction-free Bessel beam in a guided-wave configuration using a prismatic array of gold metasurface with a footprint of only ~11 μm. By locally engineering the effective index of the waveguide via evanescent coupling to plasmonic resonators, the meta-axicon converted an incident Gaussian beam into a Bessel–Gaussian beam. In addition, Liao et al. proposed and experimentally demonstrated an AI-assisted on-chip nanophotonic convolver based on a silicon metasurface, as shown in Figure 4d [124]. By employing a genetic algorithm for inverse design, they realized a dispersionless metalens operating at dual wavelengths of 1000 and 1550 nm, with focusing efficiencies of 79% and 85%, respectively. A 4f optical processing system composed of two such metalenses was constructed to perform spatial convolution operations on arbitrary functions simultaneously at both wavelengths, achieving an average deviation of 14.2% at 1000 nm and 6.1% at 1550 nm, providing a promising scheme for on-chip all-optical computing.

Moreover, the capabilities of on-chip metasurfaces also have been extended beyond linear optics to nonlinear frequency conversion. In 2021, Wang et al. established a robust and broadband alternative to conventional nonlinear methods by patterning gradient metasurfaces composed of phased arrays of amorphous silicon nano-antennas onto lithium niobate waveguides, achieving phase-matching-free second-harmonic generation [125], as shown in Figure 4e. The design provided a unidirectional effective wavevector that broke the symmetry of nonlinear coupling, enabling a monotonic increase in the second-harmonic power over many coherence lengths without requiring traditional phase matching. This work demonstrated the potential of on-chip metasurfaces for integrated nonlinear photonic applications.

Table 3 summarizes representative in-plane guided-wave metasurface devices, comparing their phase mechanisms, tunable dimensions, efficiency/bandwidth, footprint, and static/dynamic capability. Obviously, these studies illustrate that on-chip metasurfaces offer a versatile and powerful platform for in-plane manipulation of guided waves, spanning mode conversion, polarization control, beam shaping, and nonlinear frequency conversion, all within compact footprints and with high efficiency. The progressive integration of inverse design methodologies has further expanded the functional complexity and performance of these devices, paving the way for densely integrated photonic circuits with advanced light-manipulation capabilities.

Table 3. Comparison of representative in-plane guided-wave metasurface devices (Section 4).

Ref.	Phase Mechanism	Tunable Dimensions	Efficiency /Bandwidth	Footprint	Static/ Dynamic
[109]	/	Mode	Mode purity ~95%; transmission ~88%	Nanoscale	Static
[110]	Resonant phase	Mode, polarization	/	Few wavelengths	Static
[111]	/	Mode	Insertion loss < 1 dB; crosstalk < −10 dB; 20 nm around 1550 nm	5.75/6.736 μm	Static
[68]	Resonant phase	Mode	/	/	Dynamic
[112]	Inverse design	Mode, polarization	/	2.4 × 2.4 μm^2	Static
[113]	Resonant phase	Wavelength (1.3/1.6 μm)	Extinction ratio up to 20 dB	4 × 4 μm	Static
[122]	/	Phase, wavefront	Insertion loss < 1 dB over 200 nm	/	Static
[124]	Inverse design	Wavelength (1000/1550 nm), spatial convolution	79%/85% focusing; deviation 14.2%/6.1%	/	Static
[125]	Resonant phase	Wavelength conversion	broadband	compact	Static

5. Guided-Wave Radiation Control with On-Chip Metasurfaces

5.1. On-Chip Metasurface Design with Different Mechanisms

Integrated photonics enables dense component integration on a chip but offers limited controllability over free-space light. To fully leverage photonic integrated circuits in free-space applications, an interface capable of flexibly manipulating guided-wave radiation is essential. Conventional couplers, such as edge couplers [126] and surface grating couplers [127], provide limited functionality and lack comprehensive light-field control. Metasurfaces offer a viable route toward complete control of light across integrated photonics and free-space platforms.

A straightforward approach to achieving phase modulation is the detour phase, which relies on the spatial displacement of meta-atoms within each unit cell. In 2021, Ha et al. designed a periodically arranged array of identical square nanoholes on an SOI slab waveguide, utilizing the detour phase combined with a particle swarm optimization algorithm to realize a four-channel multiplexed radiation hologram [128]. Each nanohole introduces a local phase shift through its displacement relative to the unit-cell center, and by precisely designing the position of each unit, the required phase profiles were imparted to guided waves incident from the $\pm$x and $\pm$y directions, enabling multi-functional wavefront control without complex nanostructure shapes.

An alternative mechanism is the resonant phase, which arises from the excitation of electric and magnetic dipole resonances in the meta-atoms. Unlike displacement-based approaches, Guo et al. employed metal-insulator-metal rectangular nanorod antennas on an SOI waveguide, utilizing resonant phase to control guided-wave radiation, as shown in Figure 5a [129]. By simultaneously exciting electric and magnetic dipole resonances that couple with the waveguide's evanescent field, the structure provides a discontinuous phase shift exceeding 2π for the radiated light, enabling beam deflection, focusing, and orbital angular momentum (OAM) beam generation.

A third fundamental mechanism is the geometric phase, which is induced by rotating anisotropic meta-atoms. To simplify design complexity, Fang et al. proposed a geometric-phase metasurface scheme for guided-wave radiation control, as shown in Figure 5b [130]. The intrinsic TE mode of the waveguide is decomposed into left- and right-handed circularly polarized components, and by designing rectangular Si metasurface structures with varying rotation angles on a lithium niobate on insulator slab waveguide, they achieved high signal-to-noise ratio focusing, holography, and multi-channel vortex beam generation.

Since single-phase-modulation mechanisms often support only a limited number of functions, hybrid strategies that combine multiple mechanisms have been developed to expand device diversity. One such combination involves detour and resonant phases. In 2024, Zhao et al. independently controlled TE and transverse magnetic (TM) modes using propagating phase (a form of detour phase) and resonant phase with polarization-sensitive cross-shaped metasurfaces, achieving dual-port, four-channel holographic multiplexing [131]. In the same year, Li et al. combined resonant phase for free-space incident light and propagating phase for guided-wave incident light, designing a multifunctional metasurface that supports both illumination schemes and realizes six-channel multiplexed holography [132].

Another hybrid approach combines detour and geometric phases. In 2023, Fang et al. designed a non-uniformly arranged on-chip metasurface integrating both mechanisms [133]. By introducing three structural degrees of freedom—displacement in the x- and y-directions and rotation angle—within the unit cell, they achieved three independently controlled phase channels and experimentally demonstrated polarization- and wavelength-multiplexed multi-channel holographic displays.

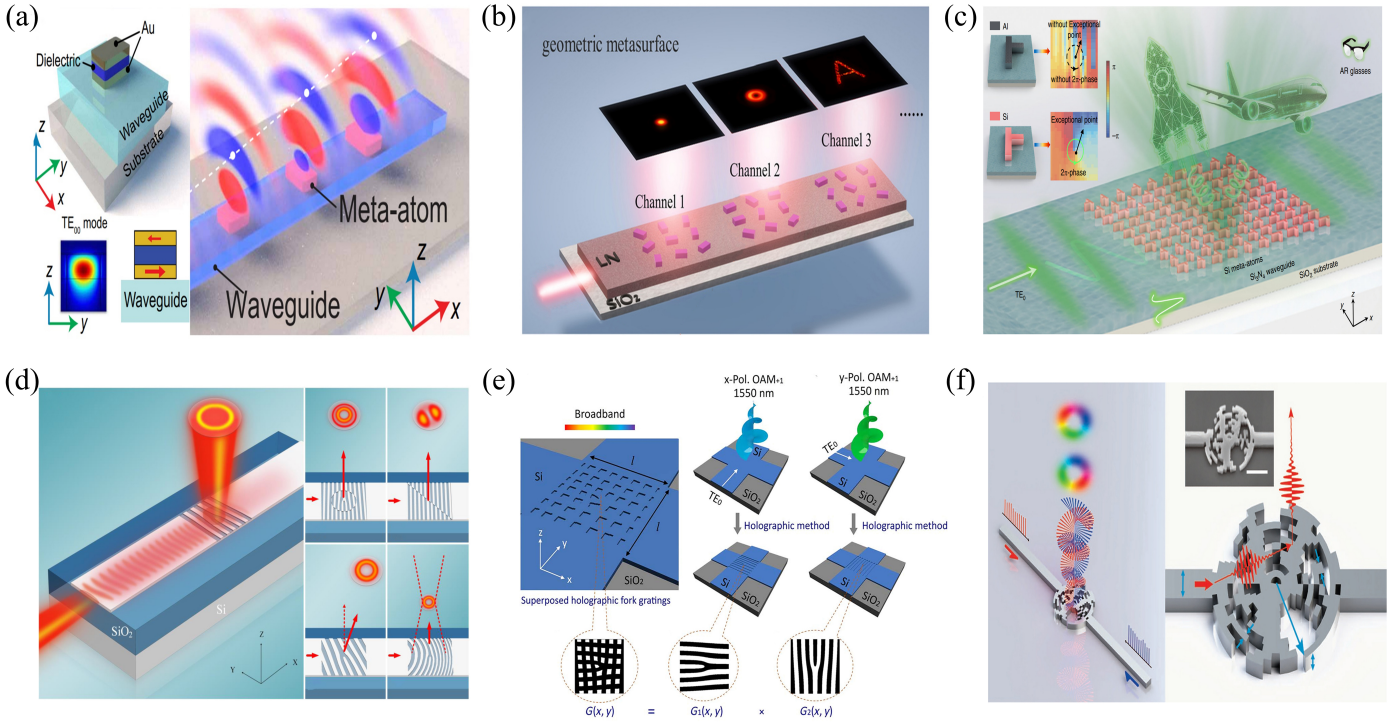


Figure 5. Modulation mechanisms of guided-wave radiation by on-chip metasurfaces. (**a**) Resonant phase. Reprinted from [129] under a Creative Commons Attribution NonCommercial License 4.0 (CC BY-NC). Copyright © 2020 The Authors; (**b**) Geometric phase [130]; (**c**) Topological phase combined with geometric phase [134]; (**d**) Subwavelength holographic grating metasurface [135]; (**e**) Superposed holographic fork grating metasurface. Reprinted from [136] under a Creative Commons Attribution NonCommercial License 4.0 (CC BY-NC). Copyright © 2019 The Authors; (**f**) Complex metasurface based on inverse design [137]. The figure illustrates the evolution from single-mechanism phase modulation to hybrid multiplexing strategies and advanced inverse-designed structures, demonstrating progressively increasing functionality and multiplexing capacity.

Beyond conventional phase mechanisms, topological phase has recently been introduced to on-chip metasurfaces for guided-wave radiation manipulation. In 2025, Yi et al. integrated non-Hermitian photonics with integrated photonics, proposing an all-dielectric on-chip topological metasurface, as shown in Figure 5c [134]. By tuning the geometric parameters of "T"-shaped unit cells, they created and encircled an exceptional point in the visible band to achieve a 2π topological phase accumulation. Combining this with the geometric phase enabled complete decoupling and independent control of left- and right-handed circularly polarized light, demonstrating dual-channel vector holography and augmented reality display.

In addition to periodically arranged metasurfaces, disordered aperiodic subwavelength structures have also been explored as generalized metasurfaces for guided-wave radiation control. In 2019, Zhou et al. used superimposed holographic fork gratings as subwavelength surface structures to demonstrate an ultra-compact, broadband, polarization-diverse silicon-based OAM beam generator, achieving efficient coupling from waveguide modes to free-space OAM modes, as shown in Figure 5d [135]. Subsequently, Zheng et al. developed on-chip integrated subwavelength holographic gratings capable of generating various phase-structured beams as well as directional emission and focusing functions, as shown in Figure 5e [136].

Moreover, inverse design has emerged as a powerful approach to create complex, aperiodic metasurface patterns that are difficult to conceive through traditional forward design. Unlike conventional methods, Xie et al. divided the nanostructure region into 288 pixels and, using simulated annealing and genetic algorithms, iteratively optimized to obtain a complex aperiodic 2D metasurface pattern, achieving ultra-broadband, high-performance OAM emission, as shown in Figure 5f [137].

5.2. Multifunctional and Multiplexed On-Chip Metasurface

To expand the functionality of on-chip devices, a wider range of degrees of freedom can be exploited for multidimensional manipulation of guided-wave radiation, including the wavelength, mode, and incident direction of the input guided waves, as well as the polarization state, diffraction distance, and diffraction order of the radiated light. Such multidimensional control not only significantly broadens the functional boundaries of on-chip photonic devices but also lays the foundation for highly integrated, multifunctional photonic systems.

Polarization was among the first dimensions introduced for multiplexing on on-chip metasurfaces. As shown in Figure 6a, Fang et al. leveraged the spin-decoupling property of geometric phase to encode independent phase distributions within a single metasurface, achieving dual-channel wavefront manipulation such as bifocal focusing and holographic multiplexing [138]. Afterwards, Hsieh et al. introduced the incident direction of the guided mode as a new multiplexing degree of freedom [139]. As shown in Figure 6b, the metasurface consisted of amorphous silicon nanopillars evanescently coupled to the TE_0 waveguide mode, where the emission phase was controlled by the nanopillar radius through propagation phase delay. By controlling the excitation direction of the guided mode, the focused spot could be switched between two positions with a tilt angle of -11°, achieving diffraction-limited focusing with a Strehl ratio of 0.82. An integrated meta-hologram was also experimentally realized to project an image above the chip, demonstrating the versatility of the platform for complex wavefront generation. Furthermore, by establishing a mapping between meta-atom displacement and oblique azimuthal angles and optimizing the corresponding detour phases, Zhao et al. successfully demonstrated the switching of up to six independently encoded holographic channels under illumination at six distinct azimuthal angles (ranging from 0° to 150°) [140]. This work broke through previous limitations that confined incident directions to orthogonal axes ($\pm x/\pm y$), greatly enhancing the flexibility of on-chip optical information retrieval. The combination of the above two dimensions enables a multiplication of functionalities. Deng et al. designed an on-chip metasurface based on V-shaped gold nanoantennas, ingeniously combining resonant phase and detour phase to achieve independent control over orthogonal polarization states and counter-propagating guided waves on a single straight waveguide [141]. Through different combinations of input direction and output polarization, they integrated up to four distinct functions, including switchable focusing/defocusing and the generation of OAM beams with different topological charges. In the same year, Ji et al. proposed a metacell-based on-chip metasurface integrating propagating phase, geometric phase, and resonant phase, as shown in Figure 6c [142]. Under dual-port guided-wave illumination along the +x and +y directions, they constructed an asymmetric, non-unitary equivalent Jones matrix, realizing full-parameter Jones matrix modulation. The near- and far-fields displayed eight Greek and English letters with specific polarization properties, breaking in-plane symmetry and significantly expanding multi-channel multiplexing capacity.

Meanwhile, Liu et al. proposed a spin and angle co-multiplexing method based on a k-space translation strategy, as shown in Figure 6d [143]. By superimposing the phase gradient carried by totally internally reflected light within the waveguide onto the metasurface phase modulation, they enabled six independent holographic channels to freely switch between the propagation-wave and evanescent-wave regions in k-space, achieving crosstalk-free projection display. To meet the demands of full-color augmented reality displays, Jia et al. designed a diatomic metasurface composed of orthogonal nanopillars, where the two nanopillars within each unit cell independently modulate two orthogonal linear polarization states [144]. Through precise dispersion engineering for the red, green, and blue wavelength channels, they realized high-fidelity, full-color holographic images switchable under two orthogonal polarization states. Li et al. extended the multiplexing dimension into the spatial domain by exploiting the wavelength-dependent phase accumulation during guided-wave propagation and employing a gradient descent optimization algorithm, successfully reconstructing multiple color images at three different depth planes, thereby achieving joint wavelength and diffraction distance multiplexing [145].

Going a step further, Liu et al. employed an end-to-end inverse design framework to realize triple joint multiplexing of incident direction, wavelength, and diffraction distance, enabling a single metasurface to respond to four incident directions, three color channels, and three reconstruction distances, thus constructing up to 36 independent holographic channels [146]. On this basis, Wang et al. introduced non-orthogonal incident angles as a new dimension in combination with polarization and wavelength [147]. Through a rigorous phase hybridization and encoding strategy that projects detour and geometric phases onto non-orthogonal directions, they achieved 24 independent holographic channels under six incident angles, two wavelengths, and two orthogonal circular polarization states, significantly enhancing the security of optical storage. Recently, Zhao et al. introduced the diffraction order dimension into the multiplexing framework, proposing a single-cell order-decoupling method [148]. By analyzing the mathematical relationships among the phases of different diffraction orders and optimizing the detour phase structure, they enabled independent encoding of the -1st, -2nd, and -3rd diffraction orders. Combined with detour and geometric phase modulation and meticulous dispersion engineering, they simultaneously manipulated four dimensions—wavelength, wavevector direction, polarization, and diffraction order—achieving up to 16 independent holographic channels under both on-chip and free-space incidence modes, providing a new pathway for ultra-high-capacity optical storage and encryption. Recently, Shi et al. also proposed and experimentally demonstrated an on-chip nonlocal metasurface color router based on symmetry-broken quasi-bound states in the continuum (q-BICs), as shown in Figure 6e [149]. By precisely engineering the geometric asymmetry and scaling factor of meta-diatom pairs integrated on a Si_3N_4 waveguide, they simultaneously achieved narrowband spectral extraction and intensity tuning of the out-coupled light. Through spatial mapping and cascading of distinct q-BIC-assisted meta-diatom pixels along the propagation direction, multicolor routing was realized with a significant improvement in energy utilization efficiency compared with conventional spatial-multiplexing designs.

From the simple multiplexing of single dimensions such as polarization and incident direction, to the progressive introduction and joint control of wavelength, diffraction distance, diffraction order, and other dimensions, the multifunctional and multidimensional multiplexing technologies of on-chip metasurfaces are continuously evolving toward higher information density, stronger security, and richer functionalities.

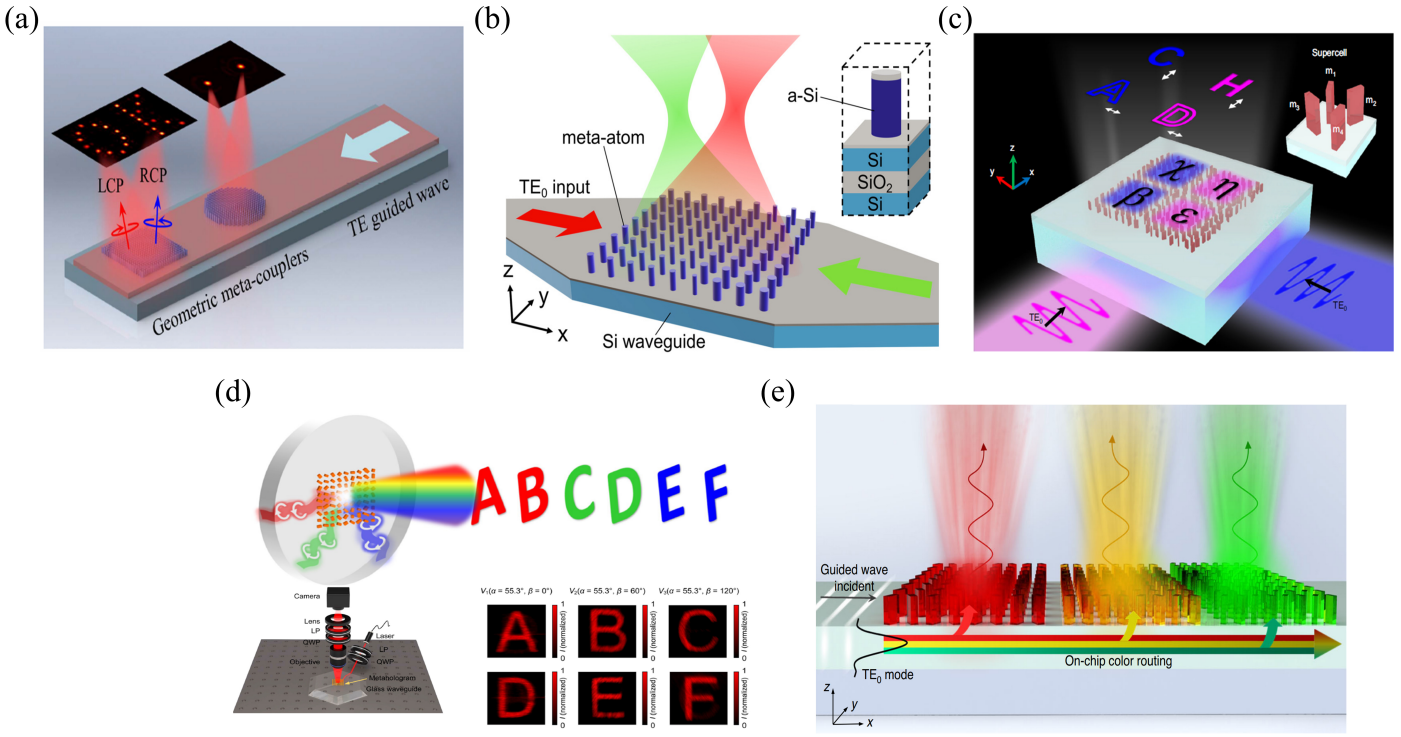


Figure 6. On-chip metasurfaces for multifunctional and multidimensional multiplexing. (**a**) Polarization multiplexing [138]; (**b**) Incident direction multiplexing [139]; (**c**) Joint multiplexing of incident direction and polarization. Reprinted from [142] under a Creative Commons Attribution-NonCommercial-NoDerivatives 4.0 International License (CC BY-NC-ND). Copyright © 2024, The Author(s); (**d**) Joint multiplexing of incident direction and wavelength [143]; (**e**) on-chip multiplexed color routers through spatial mapping and cascading of metasurface [149].

5.3. Dynamic Wavefront Manipulation with On-Chip Metasurfaces

Significant progress has been achieved in static light-field manipulation using on-chip metasurfaces. However, to meet the growing demand for real-time and reconfigurable optical applications, dynamic tunability has become a critical frontier in on-chip metasurface research [150,151]. By introducing external stimuli such as humidity [152,153], thermal effects [154,155], and electrical fields [156–158], real-time and dynamic control over the radiated light field can be realized, thereby expanding the application potential in dynamic displays, reconfigurable optical systems, optical communications, and beyond.

In 2023, to address the limited field of view (FOV) of optical phased arrays (OPA), Wang et al. integrated a metasurface doublet with a port-selected OPA on the lithium niobate on insulator (LNOI) platform, as shown in Figure 7a [150]. By cascading convex and concave quadratic-phase metasurface lenses to form a Galilean telescope configuration, they achieved a 1.54-fold FOV magnification at 1550 nm with a diffraction efficiency exceeding 41%, providing a compact solution for wide-angle beam steering in solid-state LiDAR. As an alternative, Li et al. exploited the natural humidity-responsive properties of hydrogel materials [153]. Through a single-step electron-beam lithography process, they fabricated a waveguide-type metasurface with embedded nanogrooves on a polyvinyl alcohol (PVA) thin film. By adjusting humidity through a simple exhalation process, the hydrogel waveguide underwent swelling or shrinking, thereby modifying the optical extraction efficiency of the local nanogrooves. This enabled ON/OFF switching of optically concealed information and dynamic switching between dual-channel holographic images within 310 ms. Furthermore, by utilizing the wavelength-angle dispersion relation, they encrypted and demonstrated color-mixed holographic images under specific humidity conditions. Although humidity-driven modulation suffers from relatively slow

response speeds, its advantages—requiring no external power supply and involving a simple fabrication process—make it particularly attractive for wearable and single-use encryption devices.

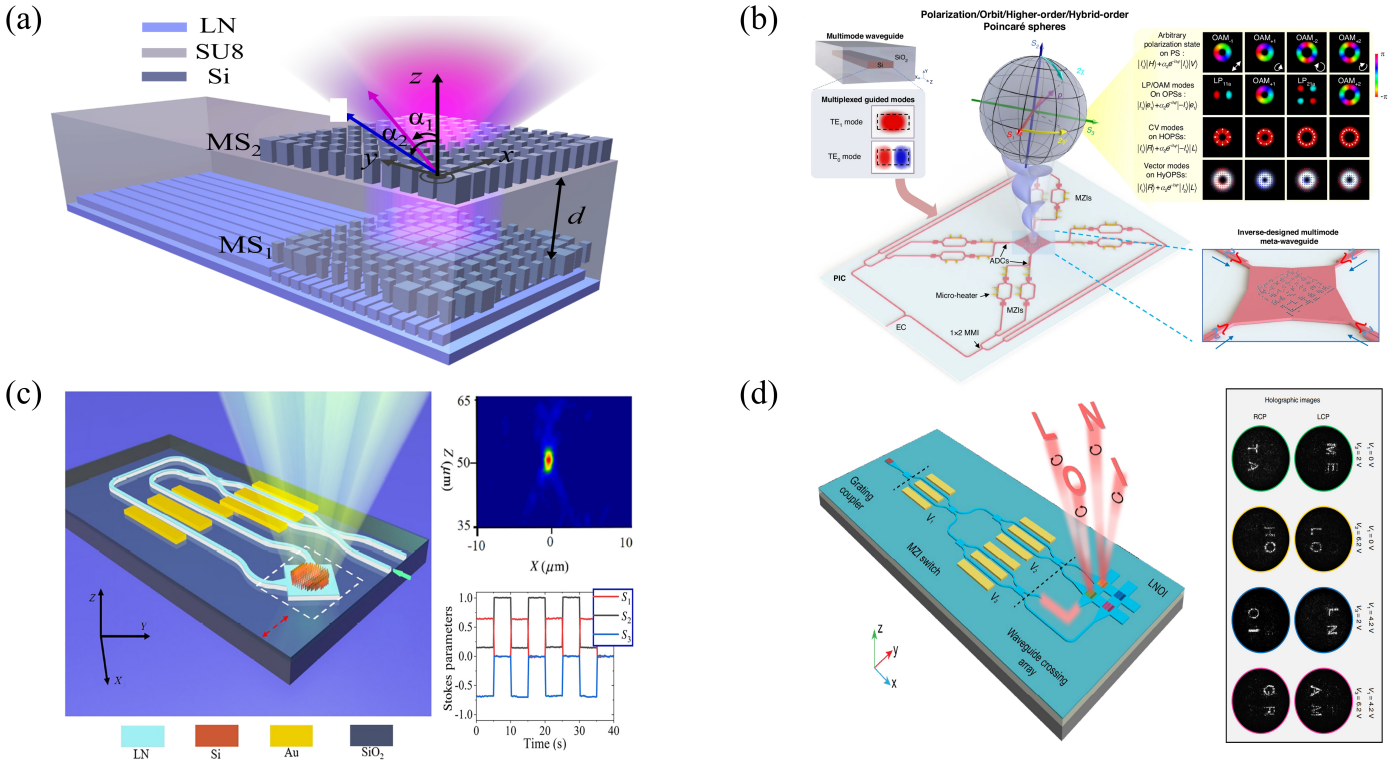


Figure 7. Dynamic wavefront manipulation based on on-chip metasurface. (**a**) Dynamic beam steering enabled by integration of optical phased array with metasurface [150]; (**b**) Tunable and versatile Poincaré sphere beam generation based on silicon thermo-optic modulation [155]; (**c**) High-speed switchable wavefront shaping based on lithium niobate electro-optic modulation [157]; (**d**) Nanosecond-scale dynamic holographic switching based on lithium niobate electro-optic modulation [158].

For more complex structured light generation, Zheng et al. proposed a fully tunable Poincaré sphere beam generator based on an eight-channel space-multiplexed multimode silicon photonic integrated circuit, as shown in Figure 7b [155]. The chip densely integrates mode multiplexers, amplitude–phase modulators, and an inversely designed multimode meta-waveguide. The multimode meta-waveguide, featuring a photonic-crystal-like pixelated structure optimized via a direct-binary-search inverse algorithm, achieves high-purity, broadband one-to-one mapping between eight on-chip guided modes (TE_0/TE_1 from four directions) and eight OAM modes with distinct polarizations and topological charges within an ultra-compact footprint of 3.6 × 3.6 μm^2. By synergistically controlling the amplitude and phase of sixteen thermo-optic modulation channels, this device achieves, for the first time on a single photonic chip, full-field manipulation of OAM mode bases. Consequently, it enables continuous mapping of arbitrary scalar, vectorial, and hybrid modes across more than eight distinct Poincaré spheres—including the fundamental Poincaré sphere, OAM Poincaré sphere, higher-order Poincaré sphere, and hybrid-order Poincaré sphere—with further scalability to higher-dimensional Poincaré hyperspheres within four-dimensional Hilbert space. Complementary to these approaches, in 2024, Shi et al. integrated an on-chip diatomic metasurface with an electrically driven liquid crystal platform [156]. By independently controlling the displacements and orientation angles of two orthogonal nanopillars within each unit cell, they achieved simultaneous

modulation of arbitrary polarization states and phases of the emitted light, reconstructing up to nine-channel fully polarized vectorial holograms. Leveraging the electro-optic response of liquid crystals, holographic images floating in real-world backgrounds could be dynamically switched in real time under voltage control, offering an electrically driven solution for wearable augmented reality displays.

To further enhance modulation speed and addressability, researchers have turned to lithium niobate platforms, which possess excellent electro-optic coefficients. Zhong et al. integrated metasurfaces with Mach–Zehnder interferometers and phase shifter electrodes on thin-film LN photonic integrated circuits, as shown in Figure 7c [157]. Through electro-optic modulation, they independently controlled the amplitude and phase of two orthogonally propagating TE_0 modes, achieving arbitrary reconstruction of output polarization states on the Poincaré sphere, dynamic switching of focal spot lateral positions and focal lengths, as well as switchable generation of OAM and Bessel beams, with a modulation bandwidth reaching 1.4 GHz. Building upon this, Ji et al. constructed an addressable on-chip metasurface network based on a 2×2 LN waveguide crossing array, as shown in Figure 7d [158]. By employing joint modulation of geometric phase and detour phase, each unit cell was designed as a basic addressing element. A two-stage LN switch, consisting of three Mach–Zehnder modulators, controlled the optical routing of four input ports, successfully demonstrating nanosecond-response dynamic addressing and switching among eight holographic images. This work overcome previous limitations of global modulation and showcased a scalable architecture for pixel-level high-speed control.

These studies demonstrate that dynamic control of on-chip metasurfaces is rapidly evolving from simple ON/OFF switching of single functions toward multidimensional addressable manipulation, ultrafast response, and reconfigurable generation of complex structured light fields, providing critical technological support for on-chip integration in high-speed optical communications, quantum information processing, dynamic displays, and sensing applications. For comparison, several representative guided-wave radiation control devices are summarized in Table 4.

Table 4. Comparison of representative guided-wave radiation control devices (Section 5).

Ref.	Phase Mechanism	Tunable Dimensions	Efficiency /Bandwidth	Footprint	Static/ Dynamic
[128]	Detour phase	Incident direction	/	/	Static
[129]	Resonant phase	Phase, OAM	/	/	Static
[130]	Geometric Phase	Spin, OAM	/	/	Static
[134]	Topological/ geometric	Spin, vector holography	/	/	Static
[135]	Holographic grating	OAM, polarization diversity	Efficient; broadband	$3.6 \times 3.6\ \mu m^2$	Static
[137]	Inverse design	OAM	High-performance; ultra-broadband	288 pixels	Static
[146]	Inverse design	Incident direction, wavelength, diffraction distance	/	/	Static
[148]	Detour/geometric	Wavelength, wavevector direction, polarization, diffraction order	/	/	Static

Table 4. *Cont.*

Ref.	Phase Mechanism	Tunable Dimensions	Efficiency /Bandwidth	Footprint	Static/ Dynamic
[150]	Combined Phase	Phase, beam steering	/	Compact	Dynamic
[153]	detour	Humidity	/		Dynamic
[155]	Inverse design	Mode, polarization, OAM	High-purity; broadband	$3.6 \times 3.6\ \mu m^2$	Dynamic
[157]	Resonant/detour	Amplitude, phase, polarization, OAM	1.4 GHz modulation	/	Dynamic
[158]	Geometric/detour	Amplitude, phase, polarization, holography	Nanosecond response		Dynamic

6. Conclusions and Prospects

In this review, we have systematically investigated the recent progress in on-chip metasurfaces for versatile light field manipulation, with a particular focus on guided-wave radiation control. We first elucidated the fundamental phase modulation mechanisms—resonant phase, geometric phase, detour phase, hybrid strategies, and inverse design—that collectively provide a versatile toolbox for tailoring light fields at subwavelength scales. We then examined the three core application scenarios: free-space-to-chip coupling, in-plane guided-wave manipulation, and guided-wave-to-free-space radiation. For coupling applications, we highlighted how metasurfaces overcome the intrinsic limitations of conventional grating and edge couplers, enabling broadband, polarization-insensitive, and angle-tolerant interfaces that efficiently bridge the gap between free-space optics and on-chip waveguides. For in-plane manipulation, we reviewed the transformative role of metasurfaces in mode conversion, polarization management, beam shaping, and nonlinear frequency conversion, demonstrating their capacity to replace or augment traditional bulky optical elements with compact, lithographically defined nanostructures. For guided-wave radiation control, we presented a comprehensive framework that traces the evolution from single-mechanism phase modulation to hybrid multiplexing strategies, and from static wavefront shaping to dynamic, reconfigurable control. These developments highlight the growing sophistication of on-chip metasurfaces and their potential to reshape integrated photonics.

Looking forward, several key challenges and opportunities merit attention.

- Efficiency and loss. On-chip metasurfaces offer a compact route to bridge guided waves and free-space waves with arbitrary wavefront control. However, the most critical bottleneck is the intrinsic trade-off between strong field confinement and efficient radiative outcoupling. In practice, extraction efficiency is limited by phase matching, mode overlap, impedance mismatch, and material absorption. Overcoming this bottleneck requires inverse-designed meta-atoms, low-loss material platforms (e.g., SiN and LNOI), and hybrid dielectric–plasmonic or ENZ-assisted designs that decouple confinement from loss.
- Dynamic tunability. Real-time reconfigurable wavefront manipulation is essential for dynamic displays, LiDAR, optical communications, and adaptive photonic circuits. The most critical bottleneck is achieving high-speed, low-loss, low-power, and large-modulation-depth tuning simultaneously. Thermo-optic tuning is slow, electro-optic tuning often requires high voltage and introduces additional loss, and phase-change or liquid-crystal approaches face trade-offs in cyclability and speed. Promising solutions include heterogeneous integration with lithium niobate, graphene, 3D Dirac semimetals, and other low-loss tunable materials, together with optimized electrode and cavity designs.

- Scalable fabrication. Moving from proof-of-concept devices to practical systems requires large-area, high-throughput, and low-cost fabrication [159–162]. The most critical bottleneck is maintaining sub-100 nm feature resolution, high uniformity, and accurate overlay over large areas. Electron-beam lithography is serial and expensive, while deep-ultraviolet lithography and nanoimprint still face challenges in overlay accuracy, mold fabrication, and compatibility with complex 3D geometries. Two-photon 3D printing and other additive approaches may complement conventional lithography, but their resolution–throughput trade-off remains to be resolved.
- Intelligent inverse design. Algorithm-driven inverse design can discover non-intuitive structures and expand the functionality of on-chip metasurfaces. The most critical bottleneck is not the optimization itself, but the lack of fabrication-aware, robust, and interpretable design. Many inverse-designed structures contain features that are difficult to fabricate, sensitive to disorder, or poorly generalizable across platforms. Future progress requires physics-informed machine learning, multi-objective optimization, fabrication-constrained parameterization, and digital or quantized metamaterial representations.
- Multidimensional multiplexing and topological light fields. Multidimensional multiplexing and topological/singular light fields provide extra degrees of freedom for high-capacity storage, encryption, and robust optical encoding [163–165]. The most critical bottleneck is inter-channel crosstalk and mode matching between free-space topological or singular fields and guided modes on chip. Hybrid multiplexing, non-Hermitian engineering, and topological metasurfaces may offer viable solutions.
- On-chip quantum metasurfaces. On-chip quantum metasurfaces could enable scalable quantum photonic circuits, deterministic single-photon manipulation, and chip-integrated quantum light sources [166–168]. The most critical bottleneck is loss and decoherence: even small propagation and scattering losses can destroy quantum states, while deterministic coupling between single-photon emitters and metasurface modes remains challenging. Low-loss platforms, cryogenic-compatible materials, heterogeneous integration, and inverse-designed quantum circuits are promising routes.

We anticipate that continued advances in materials, nanofabrication, computational design, and heterogeneous integration will propel on-chip metasurfaces toward widespread implementation in next-generation communication, sensing, display, and information processing systems.

Author Contributions: Conceptualization, B.F.; methodology, Y.P., M.W. and X.L.; validation, T.Z. and B.F.; investigation, Y.P. and J.C.; writing—original draft preparation, Y.P. and S.L.; writing—review and editing, J.C. and B.F.; supervision, B.F. All authors have read and agreed to the published version of the manuscript.

Funding: This work was supported by the National Natural Science Foundation of China (No. 12204446), and the Project of the College Students' Scientific and Technological Innovation Activity Program (New Talents Program) of Zhejiang Province (2026R409A07).

Data Availability Statement: No new data were created or analyzed in this study. Data sharing is not applicable to this article.

Acknowledgments: B. Fang is grateful for the support of Zhejiang Provincial Special Support Program for High-Level Talents.

Conflicts of Interest: The authors declare no conflicts of interest.

References

1. Sun, C.; Wade, M.; Lee, Y.; Orcutt, J.; Alloatti, L.; Georgas, M.; Waterman, A.; Shainline, J.; Avizienis, R.; Lin, S.; et al. Single-chip microprocessor that communicates directly using light. *Nature* **2015**, *528*, 534–538. [CrossRef] [PubMed]
2. Cheben, P.; Halir, R.; Schmid, J.; Atwater, H.; Smith, D. Subwavelength integrated photonics. *Nature* **2018**, *560*, 565–572. [CrossRef] [PubMed]
3. Marpaung, D.; Yao, J.; Capmany, J. Integrated microwave photonics. *Nat. Photonics* **2019**, *13*, 80–90. [CrossRef]
4. Bogaerts, W.; Pérez, D.; Capmany, J.; Miller, D.; Poon, J.; Englund, D.; Morichetti, F.; Melloni, A. Programmable photonic circuits. *Nature* **2020**, *586*, 207–216. [CrossRef] [PubMed]
5. Zhu, D.; Shao, L.; Yu, M.; Cheng, R.; Desiatov, B.; Xin, C.; Hu, Y.; Holzgrafe, J.; Ghosh, S.; Shams-Ansari, A.; et al. Integrated photonics on thin-film lithium niobate. *Adv. Opt. Photonics* **2021**, *13*, 242–352. [CrossRef]
6. Zhou, Z.; Ou, X.; Fang, Y.; Alkhazraji, E.; Xu, R.; Wan, Y.; Bowers, J. Prospects and applications of on-chip lasers. *eLight* **2023**, *3*, 1–25. [CrossRef]
7. Jalali, B.; Fathpour, S. Silicon photonics. *J. Light. Technol.* **2007**, *24*, 4600–4615. [CrossRef]
8. Atabaki, A.; Moazeni, S.; Pavanello, F.; Gevorgyan, H.; Notaros, J.; Alloatti, L.; Wade, M.; Sun, C.; Kruger, S.; Meng, H.; et al. Integrating photonics with silicon nanoelectronics for the next generation of systems on a chip. *Nature* **2018**, *556*, 349–354. [CrossRef] [PubMed]
9. Bogaerts, W.; Chrostowski, L. Silicon photonics circuit design: Methods, tools and challenges. *Laser Photonics Rev.* **2018**, *12*, 237–266. [CrossRef]
10. Wang, G.; Cao, W.; He, X. 3D Dirac semimetal elliptical fiber supported thz tunable hybrid plasmonic waveguides. *IEEE J. Sel. Top. Quantum Electron.* **2023**, *29*, 8400207. [CrossRef]
11. Cheng, Y.; Cao, W.; He, X. Hybrid plasmonic waveguides with tunable ENZ phenomenon supported by 3D Dirac semimetals. *Laser Photonics Rev.* **2024**, *18*, 2400167. [CrossRef]
12. Liu, Q.; Bian, Y.; Xiong, J. Progress in Passive Silicon Photonic Devices: A Review. *Photonics* **2025**, *12*, 928. [CrossRef]
13. Boes, A.; Corcoran, B.; Chang, L.; Bowers, J.; Mitchell, A. Status and potential of lithium niobate on insulator (LNOI) for photonic integrated circuits. *Laser Photonics Rev.* **2018**, *12*, 256–275. [CrossRef]
14. Zhen, W.; Wang, X.; Ding, J.; Wang, H. Controlling the symmetry of the photonic spin Hall effect by an optical vortex pair. *Phys. Rev. A* **2023**, *108*, 023514. [CrossRef]
15. Zhen, W.; Wang, X.; Ding, J.; Wang, H. Revisiting physical mechanism of longitudinal photonic spin splitting and Goos-Hänchen shift. *New J. Phys.* **2024**, *26*, 013045. [CrossRef]
16. Liu, S.; Cao, W.; Li, J.; He, X. 3d Dirac semimetal metamaterial supported terahertz tunable dual-functional polarization converter. *IEEE J. Sel. Top. Quantum Electron.* **2025**, *31*, 8500108. [CrossRef]
17. He, X.; Cao, W.; Lin, F. Tunable BIC metamaterials with Dirac semimetals. *Nanophotonics* **2025**, *14*, 4875–4925. [CrossRef] [PubMed]
18. Yu, N.; Genevet, P.; Kats, M.; Aieta, F.; Tetienne, J.; Capasso, F.; Gaburro, Z. Light propagation with phase discontinuities: Generalized laws of reflection and refraction. *Science* **2011**, *334*, 333–337. [CrossRef] [PubMed]
19. Huang, L.; Chen, X.; Mühlenbernd, H.; Li, G.; Bai, B.; Tan, Q.; Jin, G.; Zentgraf, T.; Zhang, S. Dispersionless phase discontinuities for controlling light propagation. *Nano Lett.* **2012**, *12*, 5750–5755. [CrossRef] [PubMed]
20. Zheludev, N.; Kivshar, Y. From metamaterials to metadevices. *Nat. Mater.* **2012**, *11*, 917–924. [CrossRef] [PubMed]
21. Yu, N.; Capasso, F. Flat optics with designer metasurfaces. *Nat. Mater.* **2014**, *13*, 139–150. [CrossRef] [PubMed]
22. Wang, Q.; Li, C.; Fang, B.; Ke, L.; Lu, J.; Ma, X.; Hong, Z.; Jing, X. Flexible and Independent control of asymmetric vortex beams based on spin multiplexing all dielectric metasurface. *J. Light. Technol.* **2023**, *41*, 7098–7104. [CrossRef]
23. Zeng, B.; Li, C.; Cheng, H.; Wang, L.; Jing, X.; Hong, Z.; Fang, B.; Lu, J.; Ma, X. Anisotropic programmable metasurface beam splitter based on diode real-time control. *Opt. Lasers Eng.* **2023**, *169*, 107723. [CrossRef]
24. Qin, G.; Dong, Y.; Zhang, P.; Liu, J.; Li, C.; Huang, W.; Hong, Z.; Shen, C.; Jing, X. Broadband absorber coupled with anti-reflection inverted pyramid type all-dielectric microstructure. *Opt. Lasers Eng.* **2023**, *160*, 107288. [CrossRef]
25. Sun, S.; Yang, K.; Wang, C.; Juan, T.; Chen, W.; Liao, C.; He, Q.; Xiao, S.; Kung, W.; Guo, G.; et al. High-efficiency broadband anomalous reflection by gradient metasurfaces. *Nano Lett.* **2012**, *12*, 6223–6229. [CrossRef] [PubMed]
26. Liu, Z.; Li, Z.; Liu, Z.; Li, J.; Cheng, H.; Yu, P.; Liu, W.; Tang, C.; Gu, C.; Li, J.; et al. High-performance broadband circularly polarized beam deflector by mirror effect of multinanorod metasurfaces. *Adv. Funct. Mater.* **2015**, *25*, 5428–5434. [CrossRef]
27. Tao, J.; You, Q.; Li, Z.; Luo, M.; Liu, Z.; Qiu, Y.; Yang, Y.; Zeng, Y.; He, Z.; Xiao, X.; et al. Mass-manufactured beam-steering metasurfaces for high-speed full-duplex optical wireless-broadcasting communications. *Adv. Mater.* **2021**, *34*, 2106080. [CrossRef] [PubMed]
28. Wang, S.; Wu, P.; Su, V.; Lai, Y.; Chu, C.; Chen, J.; Lu, S.; Chen, J.; Xu, B.; Kuan, C.; et al. Broadband achromatic optical metasurface devices. *Nat. Commun.* **2017**, *8*, 187–196. [CrossRef] [PubMed]

29. Liu, W.; Li, Z.; Cheng, H.; Tang, C.; Li, J.; Zhang, S.; Chen, S.; Tian, J. Metasurface enabled wide angle Fourier lens. *Adv. Mater.* **2018**, *30*, 1706368. [CrossRef] [PubMed]
30. Li, H.; Fang, B.; Chen, C.; Zhu, S.; Li, T. Cavity-enhanced metallic metalens with improved Efficiency. *Sci. Rep.* **2020**, *10*, 417–424. [CrossRef] [PubMed]
31. Arbabi, A.; Faraon, A. Advances in optical metalenses. *Nat. Photonics* **2023**, *17*, 16–25. [CrossRef]
32. Li, T.; Chen, C.; Xiao, X.; Chen, J.; Hu, S.; Zhu, S. Revolutionary meta-imaging: From superlens to metalens. *Photonics Insights* **2023**, *2*, R01. [CrossRef]
33. Zheng, G.; Muhlenbernd, H.; Kenney, M.; Li, G.; Zentgraf, T.; Zhang, S. Metasurface holograms reaching 80% efficiency. *Nat. Nanotechnol.* **2015**, *10*, 308–312. [CrossRef] [PubMed]
34. Huang, L.; Chen, X.; Mühlenbernd, H.; Zhang, H.; Chen, S.; Bai, B.; Tan, Q.; Jin, G.; Cheah, K.; Qiu, C.; et al. Threedimensional optical holography using a plasmonic metasurface. *Nat. Commun.* **2013**, *4*, 2808–2816. [CrossRef]
35. Yin, Y.; Jiang, Q.; Wang, H.; Liu, J.; Xie, Y.; Wang, Q.; Wang, Y.; Huang, L. Multi-dimensional multiplexed metasurface holography by inverse design. *Adv. Mater.* **2024**, *36*, 2312303. [CrossRef] [PubMed]
36. Zhao, R.; Huang, L.; Wang, Y. Recent advances in multi-dimensional metasurfaces holographic technologies. *PhotoniX* **2020**, *19*, 20–44. [CrossRef]
37. Almeida, E.; Bitton, O.; Prior, Y. Nonlinear metamaterials for holography. *Nat. Commun.* **2016**, *7*, 12533–12540. [CrossRef] [PubMed]
38. Li, Z.; Liu, W.; Li, Z.; Tang, C.; Cheng, H.; Li, J.; Chen, X.; Chen, S.; Tian, G. Tripling the capacity of optical vortices by nonlinear metasurface. *Laser Photonics Rev.* **2018**, *12*, 164–173. [CrossRef]
39. Ma, M.; Li, Z.; Liu, W.; Tang, C.; Li, Z.; Chen, H.; Li, J.; Chen, S.; Tian, J. Optical information multiplexing with nonlinear coding metasurfaces. *Laser Photonics Rev.* **2019**, *13*, 45–54. [CrossRef]
40. Hao, Z.; Liu, W.; Li, Z.; Geng, G.; Li, Z.; Wang, Y.; Cheng, H.; Ahmed, H.; Chen, X.; Li, J.; et al. Full complex-amplitude modulation of second harmonic generation with nonlinear metasurfaces. *Laser Photonics Rev.* **2021**, *15*, 207–215. [CrossRef]
41. Li, G.; Zhang, S.; Zentgraf, T. Nonlinear photonic metasurfaces. *Nat. Rev. Mater.* **2017**, *2*, 17010. [CrossRef]
42. Qin, J.; Jiang, S.; Wang, Z.; Cheng, X.; Li, B.; Shi, Y.; Tsai, D.; Liu, A.; Huang, W.; Zhu, W. Metasurface micro/nano-optical sensors: Principles and applications. *ACS Nano* **2022**, *16*, 11598–11618. [CrossRef] [PubMed]
43. Khan, S.; Khan, N.; Xie, Y.; Abbas, M.; Rauf, M.; Mehmood, I.; Runowski, M.; Agathopoulos, S.; Zhu, J. Optical sensing by metamaterials and metasurfaces: From physics to biomolecule detection. *Adv. Opt. Mater.* **2022**, *10*, 500–526. [CrossRef]
44. Kim, H.; Yun, H.; Jeong, S.; Lee, S.; Cho, E.; Rho, J. Optical metasurfaces for biomedical imaging and sensing. *ACS Nano* **2025**, *19*, 3085–3114. [CrossRef] [PubMed]
45. Sun, J.; Li, F.; Yan, S.; Shuai, S.; Zhu, Y.; Wang, X.; He, J.; Ni, D.; Wang, L.; Lin, S.; et al. Ultrasensitive biosensing by radiative Q-factor modulation in strongly coupled three-dimensional bound-state-in-the-continuum metasurfaces. *Nat. Photonics* **2026**, *20*, 818–828. [CrossRef]
46. Liao, K.; Gan, T.; Hu, X.; Gong, Q. On-chip nanophotonic devices based on dielectric metasurfaces. *Acta Opt. Sin.* **2021**, *41*, 0823001. [CrossRef]
47. Wang, Y.; Zhang, Y.; Cheng, H.; Chen, S. Light field manipulation based on on-chip integrated artificial microstructures (Invited). *Acta Opt. Sin.* **2024**, *44*, 1026004.
48. Yang, Y.; Seong, J.; Choi, M.; Park, J.; Kim, G.; Kim, H.; Jeong, J.; Jung, C.; Kim, J.; Jeon, J.; et al. Integrated metasurfaces for re-envisioning a near-future disruptive optical platform. *Light Sci. Appl.* **2023**, *12*, 152–179. [CrossRef] [PubMed]
49. Meng, Y.; Chen, Y.; Lu, L.; Ding, Y.; Cusano, A.; Fan, J.; Hu, Q.; Wang, K.; Xie, Z.; Liu, Z.; et al. Optical metawaveguides for integrated photonics and beyond. *Light Sci. Appl.* **2021**, *10*, 235–279. [CrossRef] [PubMed]
50. Chen, Y.; Pan, W.; Jin, X.; He, Q.; Zhou, L.; Sun, S. Far-field radiation manipulations of on-chip optical near-fields. *Opto-Electron Eng.* **2023**, *50*, 230173.
51. Yang, L.; Zou, Y. On-chip metasurfaces based on guided-mode radiation control: Progress and challenges. *Opto-Electron Eng.* **2026**, *53*, 250230.
52. Jin, X.; Sun, S.; Wang, Z.; Zhou, L. Recent progress in on-chip metasurfaces for controlling surface wave radiation (Invited). *Acta Opt. Sin.* **2026**, *46*, 0323002.
53. Wang, Z.; Fang, B.; Ji, J.; Zhu, S.; Li, T. Metasurface-empowered manipulation of light field of guided-wave radiation (Invited). *Acta Opt. Sin.* **2026**, *46*, 0323007.
54. Li, H.; Wang, C.; Cai, Y.; Zhao, T.; Gao, S.; Yue, W.; Gu, X.; Liang, J.; Hu, H.; Luo, Y.; et al. Metasurface-empowered integrated silicon photonics: Foundational principles, representative applications, and fabrication strategies. *Adv. Photonics* **2026**, *8*, 024003. [CrossRef]
55. Bernal, A.; Kwadrin, A.; Koenderink, A. Plasmonic antennas hybridized with dielectric waveguides. *ACS Nano* **2012**, *6*, 10156–10167. [CrossRef] [PubMed]

56. Guo, R.; Decker, M.; Staude, I.; Neshev, D.; Kivshar, Y. Bidirectional waveguide coupling with plasmonic Fano nanoantennas. *Appl. Phys. Lett.* **2014**, *105*, 053114. [CrossRef]
57. Chen, Y.; Zheng, X.; Zhang, X.; Pan, W.; Wang, Z.; Li, S.; Dong, S.; Liu, F.; He, Q.; Zhou, L.; et al. Efficient meta-couplers squeezing propagating light into on-chip subwavelength devices in a controllable way. *Nano Lett.* **2023**, *23*, 3326–3333. [CrossRef] [PubMed]
58. Pors, A.; Bozhevolnyi, S. Waveguide metacouplers for in-plane polarimetry. *Phys. Rev. Appl.* **2016**, *5*, 064015. [CrossRef]
59. Yao, C.; Wang, Y.; Zhang, J.; Zhang, X.; Zhao, C.; Wang, B.; Singh, S.; Guo, C. Dielectric nanoaperture metasurfaces in silicon waveguides for efficient and broadband mode conversion with an ultrasmall footprint. *Adv. Opt. Mater.* **2020**, *8*, 2000529. [CrossRef]
60. Xiang, J.; Tao, Z.; Li, X.; Zhao, Y.; He, Y.; Guo, X.; Su, Y. Metamaterial-enabled arbitrary on-chip spatial mode manipulation. *Light Sci. Appl.* **2022**, *11*, 168. [CrossRef] [PubMed]
61. Wang, Z.; Xiao, Y.; Liao, K.; Li, T.; Song, H.; Chen, H.; Uddin, S.; Mao, D.; Wang, F.; Zhou, Z.; et al. Metasurface on integrated photonic platform: From mode converters to machine learning. *Nanophotonics* **2022**, *11*, 3531–3546. [CrossRef] [PubMed]
62. Piggott, A.; Lu, J.; Lagoudakis, K.; Petykiewicz, J.; Babinec, T.; Vuckovic, J. Inverse design and demonstration of a compact and broadband on-chip wavelength demultiplexer. *Nat. Photonics* **2015**, *9*, 374–377. [CrossRef]
63. Su, L.; Piggott, A.; Sapra, N.; Petykiewicz, J.; Vuckovic, J. Inverse design and demonstration of a compact on-chip narrowband three-channel wavelength demultiplexer. *ACS Photonics* **2018**, *5*, 301–305. [CrossRef]
64. Zarei, S.; Marzban, M.; Khavasi, A. Integrated photonic neural network based on silicon metalines. *Opt. Express* **2020**, *28*, 36668–36684. [CrossRef] [PubMed]
65. Wang, Z.; Chang, L.; Wang, F.; Li, T.; Gu, T. Integrated photonic metasystem for image classifications at telecommunication wavelength. *Nat. Commun.* **2022**, *13*, 2131. [CrossRef] [PubMed]
66. Fu, T.; Zang, Y.; Huang, Y.; Du, Z.; Huang, H.; Hu, C.; Chen, M.; Yang, S.; Chen, H. Photonic machine learning with on-chip diffractive optics. *Nat. Commun.* **2023**, *14*, 70. [CrossRef] [PubMed]
67. Huang, Y.; Liu, W.; Sun, R.; Fu, T.; Wang, Y.; Huang, Z.; Yang, S.; Chen, H. Diffraction-driven parallel convolution processing with integrated photonics. *Laser Photonics Rev.* **2025**, *19*, 2400972. [CrossRef]
68. Wu, C.; Yu, H.; Lee, S.; Peng, R.; Takeuchi, I.; Li, M. Programmable phase-change metasurfaces on waveguides for multimode photonic convolutional neural network. *Nat. Commun.* **2021**, *12*, 96. [CrossRef] [PubMed]
69. Zhang, Y.; Li, Z.; Liu, W.; Cheng, H.; Choi, D.; Tian, J.; Chen, S. On-chip multidimensional manipulation of far-field radiation with guided wave-driven metasurfaces. *Laser Photonics Rev.* **2023**, *17*, 2300109. [CrossRef]
70. Wang, Z.; Song, W.; Chen, Y.; Fang, B.; Ji, J.; Xin, H.; Zhu, S.; Li, T. Metasurface empowered lithium niobate optical phased array with an enlarged field of view. *Photonics Res.* **2022**, *10*, B23–B29. [CrossRef]
71. Lee, W.; Im, C.; Zhou, C.; Bhandari, B.; Choi, D.; Lee, S. Metasurface doublet-integrated bidirectional grating antenna enabling enhanced wavelength-tuned beam steering. *Photonics Res.* **2022**, *10*, 248–255. [CrossRef]
72. Ha, Y.; Guo, Y.; Pu, M.; Zhang, F.; Li, X.; Ma, X.; Xu, M.; Luo, X. Minimized two- and four-step varifocal lens based on silicon photonic integrated nanoapertures. *Opt. Express* **2020**, *28*, 7943–7952. [CrossRef] [PubMed]
73. Ding, Y.; Chen, X.; Duan, Y.; Huang, H.; Zhang, L.; Chang, S.; Guo, X.; Ni, X. Metasurface-dressed two-dimensional on-chip waveguide for free-space light field manipulation. *ACS Photonics* **2022**, *9*, 398–404. [CrossRef] [PubMed]
74. Xie, C.; Huang, L.; Liu, W.; Hong, W.; Ding, J.; Wu, W.; Guo, M. Bifocal focusing and polarization demultiplexing by a guided wave-driven metasurface. *Opt. Express* **2021**, *29*, 25709–25719. [CrossRef] [PubMed]
75. Tanhayivash, Y.; Soofi, H.; Nikmehr, S. Phase and amplitude gradient waveguide coupled metasurfaces. *Sci. Rep.* **2025**, *15*, 19964. [CrossRef] [PubMed]
76. Huang, Z.; Marks, D.; Smith, D. Out-of-plane computer-generated multicolor waveguide holography. *Optica* **2019**, *6*, 119–124. [CrossRef]
77. Li, Z.; Liu, Y.; Zhang, C.; Qiao, Y.; Deng, R.; Shi, Y.; Li, Z. On-chip direction-multiplexed meta-optics for high-capacity 3D holography. *Adv. Funct. Mater.* **2024**, *34*, 2312705. [CrossRef]
78. Liu, Y.; Lian, Y.; Qi, P.; Chi, C.; Cheng, D.; Wang, Y. On-chip spatial multiplexing metasurface for multi-channel optical field modulation. *Opt. Express* **2025**, *33*, 27193–27206. [CrossRef] [PubMed]
79. Ding, Y.; Yang, Q.; Li, Y.; Yang, Z.; Wang, Z.; Liang, H.; Wu, S. Waveguide-based augmented reality displays: Perspectives and challenges. *eLight* **2023**, *3*, 24. [CrossRef]
80. Gopakumar, M.; Lee, G.; Choi, S.; Chao, B.; Peng, Y.; Kim, J.; Wetzstein, G. Full-colour 3D holographic augmented-reality displays with metasurface waveguides. *Nature* **2024**, *629*, 791–797. [CrossRef] [PubMed]
81. Shi, Y.; Wan, C.; Dai, C.; Wang, Z.; Wan, S.; Zheng, G.; Zhang, S.; Li, Z. Augmented reality enabled by on-chip meta-holography multiplexing. *Laser Photonics Rev.* **2022**, *16*, 2100638. [CrossRef]
82. Shi, Y.; Wang, Z.; Dai, C.; Wan, S.; Li, Z. On-chip meticulous grayscale high-resolution meta-display. *ACS Photonics* **2024**, *11*, 1311–1317. [CrossRef]

83. Tian, Z.; Zhu, X.; Surman, P.; Chen, Z.; Sun, X. An achromatic metasurface waveguide for augmented reality displays. *Light Sci. Appl.* **2025**, *14*, 94. [CrossRef] [PubMed]
84. Wan, S.; Qu, K.; Shi, Y.; Li, Z.; Wang, Z.; Dai, C.; Tang, J.; Li, Z. Multidimensional encryption by chip-integrated metasurfaces. *ACS Nano* **2024**, *18*, 18693–18700. [CrossRef] [PubMed]
85. Huang, Q.; Wang, Z.; Shi, Y.; Xu, C.; Li, Z. Toward ultra-high-capacity meta-optics storage: 3D data cube encrypted via arbitrary spatial coordinates. *Adv. Funct. Mater.* **2026**, *36*, e12017. [CrossRef]
86. Li, S.; Tsakmakidis, K.; Jiang, T.; Shen, Q.; Zhang, H.; Yan, J.; Sun, S.; Shen, L. Unidirectional guided-wave-driven metasurfaces for arbitrary wavefront control. *Nat. Commun.* **2024**, *15*, 5992. [CrossRef] [PubMed]
87. Yulaev, A.; Zhu, W.; Zhang, C.; Westly, D.; Lezec, H.; Agrawal, A.; Aksyuk, V. Metasurface-integrated photonic platform for versatile free-space beam projection with polarization control. *ACS Photonics* **2019**, *6*, 2902–2909. [CrossRef]
88. Huang, H.; Overvig, A.; Xu, Y.; Malek, S.; Tsai, C.; Alu, A.; Yu, N. Leaky-wave metasurfaces for integrated photonics. *Nat. Nanotechnol.* **2023**, *18*, 580–588. [CrossRef] [PubMed]
89. Shen, B.; Wang, P.; Polson, R.; Menon, R. Integrated metamaterials for efficient and compact free-space-to-waveguide coupling. *Opt. Express* **2014**, *22*, 27175–27182. [CrossRef] [PubMed]
90. Chen, T.; Xu, M.; Pu, M.; Zeng, Q.; Zheng, Y.; Xiao, Y.; Ha, Y.; Guo, Y.; Zhang, F.; Chi, N.; et al. Freeform metasurface-assisted waveguide coupler for guided wave polarization manipulation and spin–orbit angular momentum conversion. *ACS Photonics* **2024**, *11*, 1051–1059. [CrossRef]
91. Sun, A.; Xing, S.; Deng, X.; Shen, R.; Yan, A.; Hu, F.; Yuan, Y.; Dong, B.; Zhao, J.; Huang, O.; et al. Edge-guided inverse design of digital metamaterial-based mode multiplexers for high-capacity multi-dimensional optical interconnect. *Nat. Commun.* **2025**, *16*, 2372. [CrossRef] [PubMed]
92. Cai, L.; Pan, J.; Hu, S. Overview of the coupling methods used in whispering gallery mode resonator systems for sensing. *Opt. Lasers Eng.* **2020**, *127*, 105968. [CrossRef]
93. Falek, E.; Katiyi, A.; Greenberg, Y.; Karabchevsky, A. On-chip metasurface-on-facets for ultra-high transmission through waveguides in near-infrared. *Adv. Opt. Mater.* **2021**, *9*, 2100130. [CrossRef]
94. Siampour, H.; Kumar, S.; Davydov, V.; Kulikova, L.; Agafonov, V.; Bozhevolnyi, S. On-chip excitation of single germanium vacancies in nanodiamonds embedded in plasmonic waveguides. *Light Sci. Appl.* **2018**, *7*, 61. [CrossRef] [PubMed]
95. Dolores-Calzadilla, V.; Romeira, B.; Pagliano, F.; Birindelli, S.; Higuera-Rodriguez, A.; Veldhoven, P.; Smit, M.; Fiore, A.; Heiss, D. Waveguide-coupled nanopillar metal-cavity light-emitting diodes on silicon. *Nat. Commun.* **2017**, *8*, 14323. [CrossRef] [PubMed]
96. Guo, Y.; Pu, M.; Li, X.; Ma, X.; Song, S.; Zhao, Z.; Luo, X. Chip-integrated geometric metasurface as a novel platform for directional coupling and polarization sorting by spin–orbit interaction. *IEEE J. Sel. Top. Quantum Electron.* **2018**, *24*, 4700107. [CrossRef]
97. Meng, Y.; Hu, F.; Liu, Z.; Xie, P.; Shen, Y.; Xiao, Q.; Fu, X.; Bae, S.; Gong, M. Chip-integrated metasurface for versatile and multi-wavelength control of light couplings with independent phase and arbitrary polarization. *Opt. Express* **2019**, *27*, 16425–16439. [CrossRef] [PubMed]
98. Liu, Z.; Zhang, C.; Zhu, W.; Huang, Z.; Lezec, H.; Agrawal, A.; Guo, L. Compact stereo waveguide display based on a unidirectional polarization-multiplexed metagrating in-coupler. *ACS Photonics* **2021**, *8*, 1112–1119. [CrossRef]
99. Meng, Y.; He, T.; Liu, Z.; Hu, F.; Xiao, Q.; Liu, Q.; Gong, M. Guided mode meta-optics: Metasurface-dressed waveguides for arbitrary mode couplers and on-chip OAM emitters with a configurable topological charge. *Opt. Express* **2021**, *29*, 39406–39418. [CrossRef] [PubMed]
100. Zhang, Y.; Li, Z.; Liu, W.; Li, Z.; Cheng, H.; Tian, J.; Chen, S. Multi-band on-chip photonic spin Hall effect and selective excitation of whispering gallery modes with metasurface-integrated microcavity. *Opt. Lett.* **2021**, *46*, 3528–3531. [CrossRef] [PubMed]
101. Gong, C.; Zhang, J.; He, S. Hybrid unidirectional meta-coupler for vertical incidence to a high-refractive-index waveguide in telecom wavelength. *Opt. Lett.* **2017**, *42*, 5098–5101. [CrossRef] [PubMed]
102. Guo, R.; Decker, M.; Setzpfandt, F.; Gai, X.; Choi, D.; Kiselev, R.; Chipouline, A.; Staude, I.; Pertsch, T.; Neshev, D.; et al. High-bit rate ultra-compact light routing with mode-selective on-chip nanoantennas. *Sci. Adv.* **2017**, *3*, e1700007. [CrossRef] [PubMed]
103. Lin, Z.; Chen, Y.; Rusch, L.; Shi, W. On-chip circular polarization splitter using silicon photonic nanoantenna array. *ACS Photonics* **2018**, *5*, 4338–4342. [CrossRef]
104. Zhang, Y.; Li, Z.; Liu, W.; Li, Z.; Cheng, H.; Chen, S.; Tian, J. Spin-selective and wavelength-selective demultiplexing based on waveguide-integrated all-dielectric metasurfaces. *Adv. Opt. Mater.* **2019**, *7*, 1801273. [CrossRef]
105. Meng, Y.; Liu, Z.; Xie, Z.; Wang, R.; Qi, T.; Hu, F.; Kim, H.; Xiao, Q.; Fu, X.; Wu, Q.; et al. Versatile on-chip light coupling and (de) multiplexing from arbitrary polarizations to controlled waveguide modes using an integrated dielectric metasurface. *Photonics Res.* **2020**, *8*, 564–576. [CrossRef]
106. Xie, Z.; Lei, T.; Qiu, H.; Zhang, Z.; Wang, H.; Yuan, X. Broadband on-chip photonic spin Hall element via inverse design. *Photonics Res.* **2020**, *8*, 121–126. [CrossRef]
107. Chen, T.; Xu, M.; Pu, M.; Tang, X.; Zheng, Y.; Zeng, Q.; Xiao, Y.; Ha, Y.; Guo, Y.; Zhang, F.; et al. Free-form catenary-inspired meta-couplers for ultra-high or broadband vertical coupling. *Nanophotonics* **2025**, *14*, 1145–1155. [CrossRef] [PubMed]

108. Fang, B.; Li, H.; Zhu, S.; Li, T. Second-harmonic generation and manipulation in lithium niobate slab waveguides by grating metasurfaces. *Photonics Res.* **2020**, *8*, 1296–1300. [CrossRef]
109. Ohana, D.; Desiatov, B.; Mazurski, N.; Uriel, L. Dielectric metasurface as a platform for spatial mode conversion in nanoscale waveguides. *Nano Lett.* **2016**, *16*, 7956–7961. [CrossRef] [PubMed]
110. Li, Z.; Kim, M.; Wang, C.; Han, Z.; Shrestha, S.; Overvig, A.; Lu, M.; Stein, A.; Agarwal, A.; Loncar, M.; et al. Controlling propagation and coupling of waveguide modes using phase-gradient metasurfaces. *Nat. Nanotechnol.* **2017**, *12*, 675–683. [CrossRef] [PubMed]
111. Wang, H.; Zhang, Y.; He, Y.; Zhu, Q.; Sun, L.; Su, Y. Compact silicon waveguide mode converter employing dielectric metasurface structure. *Adv. Opt. Mater.* **2019**, *7*, 1801191. [CrossRef]
112. Shen, B.; Wang, P.; Polson, R.; Menon, R. An integrated-nanophotonics polarization beamsplitter with 2.4 $\times$ 2.4 μm^2 footprint. *Nat. Photonics* **2015**, *9*, 378–382. [CrossRef]
113. Fan, Y.; Roux, X.; Lupu, A.; Lustrac, A. Ultra-compact on-chip metaline-based 1.3/1.6 µm wavelength demultiplexer. *Photonics Res.* **2019**, *7*, 359–362. [CrossRef]
114. Wang, K.; Ren, X.; Chang, W.; Lu, L.; Liu, D.; Zhang, M. Inverse design of digital nanophotonic devices using the adjoint method. *Photonics Res.* **2020**, *8*, 528–533. [CrossRef]
115. Halir, R.; Cheben, P.; Luque-González, J.; Sarmiento-Merenguel, J.; Schmid, J.; Wangüemert-Pérez, G.; Xu, D.; Wang, S.; Ortega-Moñux, A.; Molina-Fernández, Í. Ultra-broadband nanophotonic beamsplitter using an anisotropic sub-wavelength metamaterial. *Laser Photonics Rev.* **2016**, *10*, 1039–1046. [CrossRef]
116. Xu, H.; Dai, D.; Shi, Y. Ultra-broadband and ultra-compact on-chip silicon polarization beam splitter by using hetero-anisotropic metamaterials. *Laser Photonics Rev.* **2019**, *13*, 1800349. [CrossRef]
117. Hao, W.; Wang, J.; Chen, L. Plasmonic metasurfaces enabled ultra-compact broadband waveguide TM-pass polarizer. *Ann. Phys.* **2021**, *533*, 2000422. [CrossRef]
118. Fan, Y.; Roux, X.; Korovin, A.; Lupu, A.; Lustrac, A. Integrated 2D-graded index plasmonic lens on a silicon waveguide for operation in the near infrared domain. *ACS Nano* **2017**, *11*, 4599–4605. [CrossRef] [PubMed]
119. Chen, Y.; Huang, L.; Gan, L.; Li, Z. Wavefront shaping of infrared light through a subwavelength hole. *Light Sci. Appl.* **2012**, *1*, e26. [CrossRef]
120. Ha, Y.; Wang, L.; Guo, Y.; Pu, M.; Zou, F.; Li, X.; Fan, Y.; Ma, X.; Luo, X. High-fidelity mode scaling via topological-optimized on-chip metalens for compact photonic interconnection. *Light Adv. Manuf.* **2023**, *4*, 222–232. [CrossRef]
121. Yao, C.; Singh, S.; ElKabbash, M.; Zhang, J.; Lu, H.; Guo, C. Quasi-rhombus metasurfaces as multimode interference couplers for controlling the propagation of modes in dielectric-loaded waveguides. *Opt. Lett.* **2019**, *44*, 1654–1657. [CrossRef] [PubMed]
122. Wang, Z.; Li, T.; Soman, A.; Mao, D.; Kananen, T.; Gu, T. On-chip wavefront shaping with dielectric metasurface. *Nat. Commun.* **2019**, *10*, 3547. [CrossRef] [PubMed]
123. Fan, Y.; Cluzel, B.; Petit, M.; Roux, X.; Lupu, A.; Lustrac, A. 2D waveguided Bessel beam generated using integrated metasurface-based plasmonic axicon. *ACS Appl. Mater. Interfaces* **2020**, *12*, 21114–21119. [CrossRef] [PubMed]
124. Liao, K.; Gan, T.; Hu, X.; Gong, Q. AI-assisted on-chip nanophotonic convolver based on silicon metasurface. *Nanophotonics* **2020**, *9*, 3315–3322.
125. Wang, C.; Li, Z.; Kim, M.; Xiong, X.; Ren, X.; Guo, G.; Yu, N.; Lončar, M. Metasurface-assisted phase-matching-free second harmonic generation in lithium niobate waveguides. *Nat. Commun.* **2017**, *8*, 2098. [CrossRef] [PubMed]
126. Papes, M.; Cheben, P.; Benedikovic, D.; Schmid, H.; Pond, J.; Halir, R.; Ortega-Moñux, A.; Wangüemert-Pérez, G.; Ye, W.; Xu, D.; et al. Fiber-chip edge coupler with large mode size for silicon photonic wire waveguides. *Opt. Express* **2016**, *24*, 5026. [CrossRef] [PubMed]
127. Masturzo, S.; Yarrison-Rice, J.; Jackson, H.; Boyd, J. Grating couplers fabricated by electron-beam lithography for coupling free-space light into nanophotonic devices. *IEEE Trans. Nanotechnol.* **2007**, *6*, 622–626. [CrossRef]
128. Ha, Y.; Guo, Y.; Pu, M.; Li, X.; Ma, X.; Zhang, Z.; Luo, X. Monolithic-integrated multiplexed devices based on metasurface-driven guided waves. *Adv. Theory Simul.* **2021**, *4*, 2000239. [CrossRef]
129. Guo, X.; Ding, Y.; Chen, X.; Duan, Y.; Ni, X. Molding free-space light with guided wave-driven metasurfaces. *Sci. Adv.* **2020**, *6*, eabb4142. [CrossRef] [PubMed]
130. Fang, B.; Wang, Z.; Gao, S.; Zhu, S.; Li, T. Manipulating guided wave radiation with integrated geometric metasurface. *Nanophotonics* **2022**, *11*, 1923–1930. [CrossRef] [PubMed]
131. Zhao, K.; Ha, Y.; Guo, Y.; Pu, M.; Fan, Y.; Li, X.; Zou, F.; Wang, L.; She, S.; Luo, X. On-chip integrated metasurface empowered multi-channel multiplexed three-dimensional hologram. *Adv. Opt. Mater.* **2024**, *12*, 2303009. [CrossRef]
132. Li, W.; Zhou, Y.; Ye, C.; Yan, D.; Xiong, B.; Gao, H.; Chu, T.; Ma, W. Multifunctional metasurface for simultaneous light manipulation under both guided-wave and free-space incidence. *ACS Photonics* **2024**, *11*, 1724–1733. [CrossRef]
133. Fang, B.; Shu, F.; Wang, Z.; Ji, J.; Jin, Z.; Hong, Z.; Shen, C.; Cheng, Q.; Li, T. On-chip non-uniform geometric metasurface for multi-channel wavefront manipulations. *Opt. Lett.* **2023**, *48*, 3119–3122. [CrossRef] [PubMed]

134. Yi, C.; Wang, Z.; Shi, Y.; Wan, S.; Tang, J.; Hu, W.; Li, Z.; Zeng, Y.; Song, Q.; Li, Z. Creating topological exceptional point by on-chip all-dielectric metasurface. *Light Sci. Appl.* **2025**, *14*, 262. [CrossRef] [PubMed]
135. Zhou, N.; Zheng, S.; Cao, X.; Zhao, Y.; Gao, S.; Zhu, Y.; He, M.; Cai, X.; Wang, J. Ultra-compact broadband polarization diversity orbital angular momentum generator with 3.6 × 3.6 m^2 footprint. *Sci. Adv.* **2019**, *5*, eaau9593. [CrossRef] [PubMed]
136. Zheng, S.; Zhao, Z.; Zhang, W. Versatile generation and manipulation of phase-structured light beams using on-chip subwavelength holographic surface gratings. *Nanophotonics* **2023**, *12*, 55–70. [CrossRef] [PubMed]
137. Xie, Z.; Lei, T.; Li, F.; Qiu, H.; Zhang, Z.; Wang, H.; Min, C.; Du, L.; Li, Z.; Yuan, X. Ultra-broadband on-chip twisted light emitter for optical communications. *Light Sci. Appl.* **2018**, *7*, 18001. [CrossRef] [PubMed]
138. Fang, B.; Wang, Z.; Li, Y.; Ji, J.; Xi, K.; Cheng, Q.; Shu, F.; Jin, Z.; Hong, Z.; Zhan, C.; et al. Spin-decoupled metacoupler empowered multiplexing and multifunction of guided wave radiation. *Photonics Res.* **2023**, *11*, 2194–2201. [CrossRef]
139. Hsieh, P.; Fang, S.; Lin, Y.; Huang, W.; Shieh, J.; Yu, P.; Chang, Y. Integrated metasurfaces on silicon photonics for emission shaping and holographic projection. *Nanophotonics* **2022**, *11*, 4687–4695. [CrossRef] [PubMed]
140. Zhao, Z.; Shi, Y.; Wang, Z.; Wan, S.; Li, Z.; Li, Z. Azimuth-resolved on-chip meta-hologram. *Laser Photonics Rev.* **2025**, *19*, e01642. [CrossRef]
141. Deng, L.; Cai, Z.; Liu, Y. Functionality expansion of guided mode radiation via on-chip metasurfaces. *Nano Lett.* **2024**, *24*, 9042–9049. [CrossRef] [PubMed]
142. Ji, J.; Li, J.; Wang, Z.; Li, X.; Sun, J.; Wang, J.; Fang, B.; Chen, C.; Ye, X.; Zhu, S.; et al. On-chip multifunctional metasurfaces with full-parametric multiplexed Jones matrix. *Nat. Commun.* **2024**, *15*, 8271. [CrossRef] [PubMed]
143. Liu, Z.; Gao, H.; Ma, T.; Ray, V.; Liu, N.; Zhang, X.; Guo, L.; Zhang, C. Broadband spin and angle co-multiplexed waveguide-based metasurface for six-channel crosstalk-free holographic projection. *eLight* **2024**, *4*, 7. [CrossRef]
144. Jia, W.; Xu, C.; Li, X.; Wan, S.; Wang, Z.; Shi, Y.; Li, Z. Full-color AR holography by chip-integrated meta-optics. *Nano Lett.* **2025**, *25*, 12269–12275. [CrossRef] [PubMed]
145. Li, Z.; Shi, Y.; Dai, C.; Li, Z. On-chip-driven multicolor 3D meta-display. *Laser Photonics Rev.* **2024**, *18*, 2301240. [CrossRef]
146. Liu, X.; Ma, Z.; Zhang, D.; Bao, Q.; Liu, Z.; Xiao, J. Hypermultiplexed off-chip hologram by on-chip integrated metasurface. *Adv. Opt. Mater.* **2024**, *12*, 2401169. [CrossRef]
147. Wang, Y.; Rao, R.; Wang, Z.; Xu, C.; Shi, Y.; Wan, S.; Li, Z. Multidimensional meta-optics storage via nonorthogonal-angular guidedwave incidence. *Nano Lett.* **2025**, *25*, 11413–11419. [CrossRef] [PubMed]
148. Zhao, Z.; Wang, Z.; Shi, Y.; Wan, S.; Li, Z. Multidimensional encrypted meta-optics storage empowered by diffraction order decoupling. *Adv. Mater.* **2025**, *37*, 2570147. [CrossRef] [PubMed]
149. Shi, Y.; Wan, S.; Wang, Z.; Rao, R.; Li, Z. On-chip nonlocal metasurface for color router: Conquering efficiency-loss from spatial-multiplexing. *Light Sci. Appl.* **2026**, *15*, 66. [CrossRef] [PubMed]
150. Wang, Z.; Ji, J.; Ye, X.; Chen, Y.; Li, X.; Song, W.; Fang, B.; Chen, J.; Zhu, S.; Li, T. On-chip integration of metasurface-doublet for optical phased array with enhanced beam steering. *Nanophotonics* **2023**, *12*, 2425–2432. [CrossRef] [PubMed]
151. Fang, B.; Li, Y.; Lei, Y.; Cao, J.; Shu, F.; Zhao, T.; Zhou, S.; Jin, Z.; Shen, C.; Hong, Z.; et al. Meta-coupler empowered dynamic wavefront control with on-chip polarization reconfiguration. *Opt. Express* **2025**, *33*, 3112–3122. [CrossRef] [PubMed]
152. Yang, R.; Wan, S.; Shi, Y.; Wang, Z.; Tang, J.; Li, Z. Immersive tuning the guided waves for multifunctional on-chip metaoptics. *Laser Photonics Rev.* **2022**, *16*, 2200127. [CrossRef]
153. Li, X.; Dai, C.; Shi, Y.; Wan, S.; Li, Z.; Dai, W.; Guan, Z.; Li, Z. Hydrogel-waveguiding on-chip meta-optics for dynamic multicolor holography. *Adv. Funct. Mater.* **2024**, *34*, 2408958. [CrossRef]
154. Chang, Y.; Chul, S.; Phare, C.; Miller, S.; Shim, E.; Lipson, M. 2D beam steerer based on metalens on silicon photonics. *Opt. Express* **2021**, *29*, 854–864. [CrossRef] [PubMed]
155. Zheng, S.; Luan, J.; Wu, T.; Yi, L.; Wan, Z.; Tian, Q.; Meng, Y.; Shen, Y.; Wang, K.; Zong, L.; et al. Fully tunable on-chip meta-generator for multidimensional Poincaré sphere mapping. *Light Sci. Appl.* **2026**, *15*, 341. [CrossRef] [PubMed]
156. Shi, Y.; Dai, C.; Wan, S.; Wang, Z.; Li, X.; Li, Z. Electrical-driven dynamic augmented reality by on-chip vectorial meta-display. *ACS Photonics* **2024**, *11*, 2123–2130. [CrossRef]
157. Zhong, H.; Zheng, Y.; Sun, J.; Wang, Z.; Wu, R.; Zhang, L.; Liang, Y.; Hua, Q.; Ning, M.; Ji, J.; et al. Gigahertz-rate-switchable wavefront shaping through integration of metasurfaces with photonic integrated circuit. *Adv. Photonics* **2024**, *6*, 016005. [CrossRef]
158. Ji, J.; Ye, Z.; Wang, Z.; Sun, J.; Li, X.; Li, J.; Wang, J.; Fang, B.; Gao, Z.; Hu, S.; et al. Dynamic holographic display with addressable on-chip metasurface network based on lithium niobate photonics. *Light Sci. Appl.* **2025**, *14*, 332. [CrossRef] [PubMed]
159. Kim, J.; Rho, J. Scalable manufacturing methods of large-area metasurfaces for real-world applications. *Acc. Mater. Res.* **2026**, *7*, 636–645. [CrossRef]
160. Galarreta, C.; Zhao, Y.; Mendoza-Carreo, J.; Caicedo, J.; Wright, C.; Alonso, M.; Li, J.; Mihi, A. Reconfigurable, temperature resilient phase-change metasurfaces fabricated via high throughput nanoimprinting lithography. *Adv. Sci.* **2026**, *13*, e21515. [CrossRef] [PubMed]

161. Li, K.; Chen, J.; Li, H.; Li, A.; Hou, X.; Ma, S.; Zhao, M.; Chen, S.; Liu, Q.; Yang, D.; et al. Printable meta-assemblies enable synergetic colouration. *Nature* **2026**, *652*, 1195–1203. [CrossRef] [PubMed]
162. Hoang, T.; Park, Y.; Kim, J.; Truong, H.; Parajuli, S.; Rajasekaran, B.; Kim, K.; Kang, D.; Jeon, G.; Lee, K. 300-unit-per-second roll-to-roll manufacturing of visible metalenses. *Nature* **2026**, *652*, 1188–1194. [CrossRef] [PubMed]
163. Zhen, W.; Ren, Z.; Wang, X.; Ding, J.; Wang, H. Polarization structure transition of C-point singularities upon reflection. *Sci. China Phys. Mech. Astron.* **2025**, *68*, 244211. [CrossRef]
164. Zhen, W.; Qing, Z.; Yan, W.; Ren, Z.; Wang, X.; Wang, H.; Ding, J.; Shen, Y. Reconfiguring optical skyrmion topology in free space. *Optica* **2026**, *13*, 188–194. [CrossRef]
165. Liu, X.; Kan, Y.; Kumar, S.; Kulikova, L.; Davydov, V.; Agafonov, V.; Bozhevolnyi, S. Chip-integrated metasurface-enabled single-photon skyrmion sources. *Nat. Commun.* **2026**, *17*, 8567. [CrossRef] [PubMed]
166. Kerolos, M.; Marco, D.; Matthew, Y.; Neil, S.; Marko, L.; Federico, C. Metasurface quantum graphs for generalized Hong-Ou-Mandel interference. *Science* **2025**, *389*, 416–422. [CrossRef] [PubMed]
167. Gao, Y.; Zhong, R.; Mao, X.; Zhang, H.; Jiang, Y.; Bao, C.; Li, C.; Peng, R.; Wang, M. Interference-Induced Entanglement Engineering on a Metasurface. *Phys. Rev. Lett.* **2026**, *136*, 023601. [CrossRef] [PubMed]
168. Aharonovich, I.; Crozier, K.; Neshev, D. Programmable integrated quantum photonics. *Nat. Photonics* **2026**, *20*, 254–265. [CrossRef]

Disclaimer/Publisher's Note: The statements, opinions and data contained in all publications are solely those of the individual author(s) and contributor(s) and not of MDPI and/or the editor(s). MDPI and/or the editor(s) disclaim responsibility for any injury to people or property resulting from any ideas, methods, instructions or products referred to in the content.